

# THE NONISOTHERMAL STAGE OF MAGNETIC STAR FORMATION. I. FORMULATION OF THE PROBLEM AND METHOD OF SOLUTION

MATTHEW W. KUNZ AND TELEMACHOS CH. MOUSCHOVIAS

Departments of Physics and Astronomy, University of Illinois at Urbana-Champaign, 1002 W. Green Street, Urbana, IL 61801

Accepted November 8, 2018

## ABSTRACT

We formulate the problem of the formation and subsequent evolution of fragments (or cores) in magnetically-supported, self-gravitating molecular clouds in two spatial dimensions. The six-fluid (neutrals, electrons, molecular and atomic ions, positively-charged, negatively-charged, and neutral grains) physical system is governed by the radiative, nonideal magnetohydrodynamic (RMHD) equations. The magnetic flux is not assumed to be frozen in any of the charged species. Its evolution is determined by a newly-derived generalized Ohm's law, which accounts for the contributions of both elastic and inelastic collisions to ambipolar diffusion and Ohmic dissipation. The species abundances are calculated using an extensive chemical-equilibrium network. Both MRN and uniform grain size distributions are considered. The thermal evolution of the protostellar core and its effect on the dynamics are followed by employing the grey flux-limited diffusion approximation. Realistic temperature-dependent grain opacities are used that account for a variety of grain compositions. We have augmented the publicly-available Zeus-MP code to take into consideration all these effects and have modified several of its algorithms to improve convergence, accuracy and efficiency. Results of magnetic star formation simulations that accurately track the evolution of a protostellar fragment from a density  $\simeq 10^3 \text{ cm}^{-3}$  to a density  $\simeq 10^{15} \text{ cm}^{-3}$ , while rigorously accounting for both nonideal MHD processes and radiative transfer, are presented in a separate paper.

*Subject headings:* ISM: clouds — magnetic fields — MHD — stars: formation — radiative transfer — dust, extinction

## 1. INTRODUCTION — BACKGROUND

The formulation of a theory of star formation is a formidable task. It requires understanding of the nonlinear interactions among self-gravity, magnetic fields, rotation, chemistry (including grain effects), turbulence, and radiation. Stars form in fragments within interstellar molecular clouds, which have sizes ranging from 1 to 5 pc, masses from a few tens to  $10^5 M_{\odot}$ , mean densities  $\simeq 10^3 \text{ cm}^{-3}$ , and temperatures  $\simeq 10 \text{ K}$  (Myers 1985; Heiles 1987). Their spectral lines have Doppler-broadened linewidths that suggest supersonic (but subAlfvénic) internal motions. In the deep interiors of such clouds, high-energy cosmic rays ( $> 100 \text{ MeV}$ ) maintain a degree of ionization  $x_i \lesssim 10^{-7}$ , whereas ultraviolet (UV) ionization is responsible for a much greater degree of ionization  $x_i \gtrsim 10^{-5}$  in the outer envelopes.

### 1.1. Magnetic Fields and Star Formation

The possible importance of magnetic fields to the support of interstellar clouds and to the regulation of star formation was first studied by Chandrasekhar & Fermi (1953), Mestel & Spitzer (1956), and Mestel (1965) using the virial theorem. Similar investigations by Strittmatter (1966a,b) and Spitzer (1968) followed. Mestel (1966) calculated the magnetic forces on a spherically-symmetric, gravitationally-bound cloud. Self-consistent calculations by Mouschovias (1976a,b) produced exact equilibria of initially uniform, isothermal, magnetic clouds embedded in a hot and tenuous, electrically-conducting external medium. Mouschovias & Spitzer (1976) used these equilibrium states to find the critical mass-to-flux ratio  $(M/\Phi_B)_{\text{cr}} = 1/(63G)^{1/2}$  that must be exceeded for collapse against the magnetic forces to set in. Scott & Black (1980) performed numerical simulations of the collapse of a supercritical (as a whole) magnetic cloud. A picture of molecular clouds emerged in which magnetic fields play a central role in their support and evolution (Mouschovias 1978). To this date, magnetic braking remains the only mechanism that has been shown quantitatively to resolve the most significant dynamical problem of star formation, namely, the angular momentum problem (Mouschovias & Paleologou 1979, 1980; see also summary below).

Subsequent observations lent credence to this picture by revealing the importance of magnetic fields through both dust polarization measurements and Zeeman observations. Polarization studies have exhibited large-scale ordered magnetic fields connecting protostellar cores to their surrounding envelopes (Vrba et al. 1981; Heyer et al. 1987; Novak et al. 1989, 1997; Lai et al. 2001, 2003; Crutcher et al. 2004; Alves et al. 2008), often with an hourglass morphology (Schleuning 1998; Hildebrand et al. 1999; Girart et al. 1999; Schleuning et al. 2000; Lai et al. 2002; Cortes & Crutcher 2006; Girart et al. 2006), as predicted by the theoretical calculations (Mouschovias 1976b; Fielder & Mouschovias 1993). A large body of Zeeman observations (Crutcher & Kazès 1983; Kazès & Crutcher 1986; Troland et al. 1986; Crutcher et al. 1987; Goodman et al. 1989; Crutcher et al. 1993, 1994, 1996; Troland et al. 1996; Crutcher et al. 1999a,b; Crutcher 1999; Heiles & Crutcher 2005; Cortes et al. 2005) revealed magnetic fields in the range  $\simeq 10 - 200 \mu\text{G}$  in molecular clouds, from small isolated ones to massive star-forming ones. These values are more than sufficient to establish the importance of magnetic fields in molecular cloud dynamics.

It was recognized early on (e.g., see Babcock & Cowling 1953, p. 373) that the magnetic flux of an interstellar blob of mass comparable to a stellar mass is typically several orders of magnitude greater than that of magnetic young stars. This is the so-called

“magnetic flux problem” of star formation. It lies in the fact that substantial flux loss must take place at some stage during star formation. Ambipolar diffusion (the relative motion between plasma and neutrals) was first proposed by Mestel & Spitzer (1956) as a means by which an interstellar cloud as a whole would reduce its magnetic flux and thereby collapse. Pneuman & Mitchell (1965) undertook a detailed calculation of the collapse of such (spherical) cloud. Spitzer (1968) calculated the ambipolar-diffusion timescale by assuming that the magnetic force on the ions is balanced by the (self-)gravitational force on the neutrals. Nakano (1979) followed the quasistatic contraction of a cloud due to ambipolar diffusion using a sequence of Mouschovias’ (1976b) equilibrium states, each one of which had a smaller magnetic flux than the previous one.

A new solution for ambipolar diffusion by Mouschovias (1979) showed that the essence of this process is a redistribution of mass in the central flux tubes of a molecular cloud, rather than a loss of magnetic flux by the cloud as a whole. He found the ambipolar-diffusion timescale to be typically three orders of magnitude smaller in the interior of a cloud than in the outermost envelope, where there is a much better coupling between neutral particles and the magnetic field because of the much greater degree of ionization. This suggested naturally a self-initiated fragmentation of (or core formation in) molecular clouds on the ambipolar-diffusion timescale

$$\tau_{AD} = 1.8 \times 10^6 \left( \frac{x_i}{10^{-7}} \right) \text{ yr}$$

(Mouschovias 1979, eq. [37]). The inefficiency of star formation was thereby attributed to the self-initiated formation and contraction of molecular cloud fragments (or cores) due to ambipolar diffusion in otherwise magnetically supported clouds (Mouschovias 1976b, 1977, 1978, 1979). The *central* mass-to-flux ratio eventually exceeds its critical value for collapse,

$$\left( \frac{dm}{d\Phi_B} \right)_{c,cr} = \frac{3}{2} \left( \frac{M}{\Phi_B} \right)_{cr},$$

(see Mouschovias 1976a, eq. [44]), and dynamic contraction ensues. Detailed numerical calculations in slab (Paleologou & Mouschovias 1983; Mouschovias et al. 1985), cylindrical (Mouschovias & Morton 1991, 1992a,b), and axisymmetric geometries (Fielder & Mouschovias 1992, 1993; Ciolek & Mouschovias 1993, 1994, 1995; Basu & Mouschovias 1994, 1995a,b; Ciolek & Königl 1998; Desch & Mouschovias 2001; Tassis & Mouschovias 2005a,b, 2007a,b,c) transformed this scenario of star formation into a theory with predictive power.

### 1.2. Rotation

During the early, isothermal phase of star formation, a cloud (or a fragment) must also lose a large fraction of its angular momentum (e.g., see Spitzer 1968, p. 231). Observations show that molecular clouds and embedded fragments (or cores) rarely exhibit rotation significantly greater than that of the background medium (Goldsmith & Arquilla 1985). If angular momentum were conserved from the initial galactic rotation (i.e., starting from angular velocity  $\Omega_0 \simeq 10^{-15} \text{ s}^{-1}$  at the mean density of the interstellar medium  $\simeq 1 \text{ cm}^{-3}$ ), centrifugal forces would not allow even the formation of interstellar clouds (Mouschovias 1991, § 2). Fragmentation does not alter this conclusion (Mouschovias 1977, § 1). This is referred to as the “angular momentum problem” of star formation. As far as clouds and their cores are concerned, the angular momentum problem has been shown to be resolved by magnetic braking (i.e., the transport of angular momentum from a fragment to its surrounding medium through the propagation of torsional Alfvén waves along magnetic field lines connecting the fragment to the cloud envelope) analytically by Mouschovias & Paleologou (1979, 1980) and numerically by Basu & Mouschovias (1994, 1995a,b) and Mellon & Li (2008). Hence the centrifugal forces resulting from the cloud’s or core’s rotation have a negligible effect on the evolution of the contracting core, at least up to central densities of  $\approx 10^{14} \text{ cm}^{-3}$  (see the last paragraph of Tassis & Mouschovias 2007b).

### 1.3. Grain Effects

Interstellar grains comprise about 1% of the mass in the interstellar medium (Spitzer 1978). Baker (1979) and Elmegreen (1979) suggested that charged grains may couple to the magnetic field and thereby play a role in ambipolar diffusion and star formation. Elmegreen (1979) and Nakano & Umebayashi (1980) compared the ambipolar-diffusion timescale and the free-fall timescale and concluded that ambipolar diffusion occurs over too long a timescale (roughly 10 times greater than free-fall) to be a relevant process in star formation. Refinements by the same authors (Elmegreen 1986; Umebayashi & Nakano 1990; Nishi et al. 1991) led to similar conclusions. Through detailed numerical simulations of core formation and evolution including the effects of (negative and neutral) dust grains, Ciolek & Mouschovias (1993, 1994) found that grains lengthen the timescale for the formation of a core because of grain-neutral collisions, but cautioned that the ambipolar-diffusion timescale should not be compared to the free-fall timescale in determining its relevance in magnetically-supported clouds, as originally pointed out by Mouschovias (1977), because molecular clouds are not free-falling. Velocities characteristic of such collapse have not been observed. Ciolek & Mouschovias (1995) extended these calculations by including UV ionization and a variety of atomic metal ions ( $\text{C}^+$ ,  $\text{S}^+$ ,  $\text{Si}^+$ ,  $\text{Mg}^+$ ,  $\text{Na}^+$ ,  $\text{Fe}^+$ ). Attention was also paid to the complementary effect of protostellar evolution on the microscopic physics and chemistry (Ciolek & Mouschovias 1996, 1998).

### 1.4. MHD Waves and/or Turbulence

The extent to which turbulence (or waves) may or may not affect the evolution of a protostellar fragment has been a topic of debate for several decades, receiving increased attention in recent years (Mac Low & Klessen 2004; Mouschovias et al. 2006). A consensus has yet to be reached concerning even what causes and maintains the observed broad linewidths long thought to be indicative of supersonic turbulence (Zuckerman & Evans 1974; Arons & Max 1975; Larson 1981; Zweibel & Josafatsson 1983; Mouschovias 1987; Mouschovias & Psaltis 1995; Myers & Gammie 1999; Elmegreen & Scalo 2004; Mouschovias et al. 2006),

although Mouschovias & Psaltis (1995) and Mouschovias et al. (2006) showed quantitatively that observations contradict the key assumption of turbulence simulations, namely, that molecular clouds are magnetically supercritical by a factor 4 – 10. Despite a lack of agreement on the origin of the linewidths, analytical (Mouschovias 1991) and numerical calculations (Eng 2002; Eng & Mouschovias 2009, in preparation) have demonstrated that turbulence (or waves) plays an insignificant role in the star formation process once dynamical contraction of a fragment (or core) ensues. Observations showing narrowing and eventual thermalization of linewidths in protostellar cores (Baudry et al. 1981; Myers & Benson 1983; Myers et al. 1983; Bacmann et al. 2000) are in agreement with this conclusion and with an earlier version of it (Mouschovias 1987).

### 1.5. Radiative Transfer

During the early phases of star formation the energy produced by compressional heating is radiated away by the dust grains in the infrared. At higher densities ( $\simeq 10^{11} \text{ cm}^{-3}$ ), the core traps and retains part of this heat and its temperature begins to rise. The evolution of the temperature in this nonisothermal regime may be approximated (but substantially overestimated) by using an adiabatic equation of state (Boss 1981; Desch & Mouschovias 2001; Tassis & Mouschovias 2007a,b,c). More realistic equations of state have also been employed by, for example, Bate (1998). To accurately model the nonisothermal phase of protostellar contraction, however, one needs to include a proper treatment of radiative transfer. Early efforts to include radiative transfer in (nonmagnetic) star formation calculations were confined to the use of the diffusion approximation (Bodenheimer 1968; Larson 1969, 1972; Black & Bodenheimer 1975, 1976; Tscharnuter 1975; Yorke & Krugel 1977). While the diffusion approximation is strictly applicable only to optically thick regions, its ease of implementation and relatively low computational cost make it an attractive choice. The Eddington approximation offers a slight improvement in that it retains some of the rigor of using moments of the radiative transfer equation, while making the simplifying assumption that the radiation field is everywhere isotropic. Its use in numerical calculations of (nonmagnetic) star formation has been documented in Tscharnuter (1978), Tscharnuter & Winkler (1979), Winkler & Newman (1980a,b), Boss (1984, 1986, 1988), and Boss & Myhill (1995). By implicitly assuming that photons always travel a distance comparable to their mean-free path (even if this distance exceeds the free-flight distance  $c\Delta t$ , where  $\Delta t$  is the computational timestep), the Eddington approximation gives unphysical behavior in optically thin regions, in which the mean-free-path is huge. The result is a signal speed unbound by the speed of light, i.e., it violates causality (e.g., see § 97 of Mihalas & Mihalas 1984).

Increasing the accuracy and realism of a radiative transfer algorithm often requires making limiting assumptions about the hydrodynamics in order to make the problem tractable (e.g., Yorke 1980; Masunaga et al. 1998). A full frequency- and angle-dependent treatment of the radiation is nearly always confined to postprocessing the results of a hydrodynamic calculation (Yorke 1977; Yorke & Shustov 1981; Adams & Shu 1985, 1986) or a grey (i.e., independent of frequency) radiation hydrodynamic calculation (Boss & Yorke 1990; Bodenheimer et al. 1990). By contrast, the flux-limited diffusion (FLD) approximation (Levermore & Pomraning 1981) is a propitious compromise that retains some of the advantages of the diffusion and Eddington approximations, while preserving causality and coupling self-consistently to the hydrodynamic equations.

### 1.6. Outline

In this paper we formulate the problem of the formation and evolution of protostellar fragments (or cores) in magnetically-supported, self-gravitating molecular clouds, including the effects of both ambipolar diffusion and Ohmic dissipation (which becomes important at high densities), grain chemistry and dynamics, and radiation. Using the results of Eng (2002) and Eng & Mouschovias (2009, in preparation), and Basu & Mouschovias (1994), we may safely ignore the effects of turbulence and rotation, respectively, on the evolution of the protostellar core for the densities considered here. The physical and chemical properties of the model cloud are summarized in Section 2. The radiation magnetohydrodynamic (RMHD) equations governing the evolution of the model cloud are presented and discussed in Section 3. In Section 4 we present the chemical model used in the calculations. The physics of magnetic diffusion (ambipolar and ohmic) is handled by using a generalized Ohm’s law, which is derived in Section 5. We treat the radiative transfer using the grey FLD approximation, with realistic grain opacities accounting for a variety of grain compositions (§ 6). The numerical method of solution is discussed in Section 7. Finally, we give the simplified set of equations and a brief summary in Section 8. Details, mostly mathematical, are left for the Appendix. Results are presented in a separate paper (Kunz & Mouschovias 2009, in preparation).

## 2. BASIC PROPERTIES OF THE MODEL CLOUD

We consider a self-gravitating, magnetic, weakly-ionized model molecular cloud consisting of neutral particles ( $\text{H}_2$  with 20% He by number), ions (both molecular  $\text{HCO}^+$  and atomic  $\text{Na}^+$ ,  $\text{Mg}^+$ ,  $\text{K}^+$ ), electrons, singly negatively-charged grains, singly positively-charged grains, and neutral grains. Following Desch & Mouschovias (2001), the abundances of all species (except the neutrals) are determined from the chemical reaction network shown in Table 1 and described below in Section 4.3. Cosmic rays of energy  $\gtrsim 100 \text{ MeV}$  are mainly responsible for the degree of ionization in the cloud. Once column densities  $\gtrsim 100 \text{ g cm}^{-2}$  are achieved, cosmic rays are appreciably attenuated. At even higher densities, cosmic rays are effectively shielded and radioactive decays become the dominant source of ionization. Finally, at temperatures on the order of 1000 K or higher, thermal ionization of potassium becomes important. UV radiation provides an additional ionization mechanism, but it only affects the outer envelope of molecular clouds (Hollenbach et al. 1971; Glassgold & Langer 1974). We consider spherical grains whose radii are determined by either a uniform or an MRN (Mathis et al. 1977) size distribution. In the case of collisions of ions (molecular or atomic) with grains, we assume that the ions do not get attached to the grains, but rather that they get neutralized, with the resulting neutral particle escaping into the gas phase. Thus the total abundance of metals as well as the total  $\text{HCO}$  abundance remain constant. Grain growth is not considered here.

We follow the ambipolar-diffusion-initiated evolution of an axisymmetric two-dimensional model cloud from typical mean molecular cloud densities ( $\simeq 300 \text{ cm}^{-3}$ ) to densities characteristic of the formation of a hydrostatic protostellar core. The axis of

TABLE 1  
CHEMICAL REACTION NETWORK USED IN THE CALCULATION OF THE ABUNDANCES OF CHARGED SPECIES.

Relevant Chemical Reactions in Molecular Clouds		
Cosmic-Ray Ionization:	$\text{H}_2 + \text{CR} \rightarrow \text{H}_2^+ + \text{e}$	
	$\text{H}_2^+ + \text{H}_2 \rightarrow \text{H}_3^+ + \text{H}$	
	$\text{H}_3^+ + \text{CO} \rightarrow \text{HCO}^+ + \text{H}_2$	
Dissociative Recombination:	$\text{HCO}^+ + \text{e} \rightarrow \text{H} + \text{CO}$	
Radiative recombination: <sup>a</sup>	$\text{A}^+ + \text{e} \rightarrow \text{A}^0 + h\nu$	
Charge transfer: <sup>a</sup>	$\text{A}^0 + \text{HCO}^+ \rightarrow \text{A}^+ + \text{HCO}$	
$\text{e}^-$ attachment onto grains:	$\text{e} + \text{g}_0 \rightarrow \text{g}_-$	
	$\text{e} + \text{g}_+ \rightarrow \text{g}_0$	
Atomic-ion attachment onto grains: <sup>a</sup>	$\text{A}^+ + \text{g}_- \rightarrow \text{A}^0 + \text{g}_0$	
	$\text{A}^+ + \text{g}_0 \rightarrow \text{A}^0 + \text{g}_+$	
Molecular-ion attachment onto grains:	$\text{HCO}^+ + \text{g}_0 \rightarrow \text{HCO} + \text{g}_+$	
	$\text{HCO}^+ + \text{g}_- \rightarrow \text{HCO} + \text{g}_0$	
Charge transfer by grain-grain collisions:	$\text{g}_+^\alpha + \text{g}_-^{\alpha'} \rightarrow \text{g}_0^\alpha + \text{g}_0^{\alpha'}$	
	$\text{g}_+^\alpha + \text{g}_0^{\alpha'} \rightarrow \text{g}_0^\alpha + \text{g}_+^{\alpha'}$	

<sup>a</sup>  $\text{A}^+$  represents an atomic ion, such as  $\text{Na}^+$ ,  $\text{Mg}^+$ , and  $\text{K}^+$ , and  $\text{A}^0$  the corresponding neutral atom.

symmetry is aligned with the  $z$ -axis of a cylindrical polar coordinate system  $(r, \phi, z)$ . Isothermality is an excellent approximation for the early stages of star formation, while the density is smaller than  $\approx 10^{10} \text{ cm}^{-3}$  (Gaustad 1963; Hayashi 1966; Larson 1969). However, once the heat generated by released gravitational energy during core collapse is unable to escape freely (at a central number density of  $n_{\text{opq}} \simeq 10^7 \text{ cm}^{-3}$ ), radiative transfer calculations are employed to determine the thermal evolution of the core.<sup>1</sup> This is an improvement over previous magnetic star formation calculations to reach these densities (Desch & Mouschovias 2001; Tassis & Mouschovias 2007a,b,c), which assumed an adiabatic equation of state beyond a critical density because of the high computational expense of radiative transfer calculations. Numerical techniques and computer hardware have matured enough by now to render these once impractical calculations feasible.

### 3. THE SIX-FLUID RMHD DESCRIPTION OF MAGNETIC STAR FORMATION

The RMHD equations governing the behavior of the six-fluid system (neutrals, electrons, ions, negative, positive, and neutral grains) are:

$$\frac{\partial \rho_n}{\partial t} + \nabla \cdot (\rho_n \mathbf{v}_n) = 0, \quad (1a)$$

$$\frac{\partial (\rho_{g_-} + \rho_{g_0} + \rho_{g_+})}{\partial t} + \nabla \cdot (\rho_{g_-} \mathbf{v}_{g_-} + \rho_{g_0} \mathbf{v}_{g_0} + \rho_{g_+} \mathbf{v}_{g_+}) = 0, \quad (1b)$$

$$\frac{\partial (\rho_n \mathbf{v}_n)}{\partial t} + \nabla \cdot (\rho_n \mathbf{v}_n \mathbf{v}_n) = -\nabla P_n - \rho \nabla \psi + \frac{1}{c} \mathbf{j} \times \mathbf{B} + \frac{1}{c} \chi_{\mathcal{F}} \mathcal{F}, \quad (1c)$$

$$0 = -en_e \left( \mathbf{E} + \frac{\mathbf{v}_e}{c} \times \mathbf{B} \right) + \mathbf{F}_{\text{en}}, \quad (1d)$$

$$0 = +en_i \left( \mathbf{E} + \frac{\mathbf{v}_i}{c} \times \mathbf{B} \right) + \mathbf{F}_{\text{in}}, \quad (1e)$$

$$0 = -en_{g_-} \left( \mathbf{E} + \frac{\mathbf{v}_{g_-}}{c} \times \mathbf{B} \right) + \mathbf{F}_{g_-n} + \mathbf{F}_{g_-g_0, \text{inel}}, \quad (1f)$$

$$0 = +en_{g_+} \left( \mathbf{E} + \frac{\mathbf{v}_{g_+}}{c} \times \mathbf{B} \right) + \mathbf{F}_{g_+n} + \mathbf{F}_{g_+g_0, \text{inel}}, \quad (1g)$$

$$0 = \mathbf{F}_{g_0n} + \mathbf{F}_{g_0g_-, \text{inel}} + \mathbf{F}_{g_0g_+, \text{inel}}, \quad (1h)$$

$$\nabla \times \mathbf{B} = \frac{4\pi}{c} \mathbf{j}, \quad (1i)$$

$$\mathbf{j} = e (n_i \mathbf{v}_i - n_e \mathbf{v}_e + n_{g_+} \mathbf{v}_{g_+} - n_{g_-} \mathbf{v}_{g_-}), \quad (1j)$$

$$\frac{\partial \mathbf{B}}{\partial t} = -c \nabla \times \mathbf{E}, \quad (1k)$$

$$\nabla^2 \psi = 4\pi G \rho_n, \quad (1l)$$

$$\frac{\partial u_n}{\partial t} + \nabla \cdot (u_n \mathbf{v}_n) = -P_n \nabla \cdot \mathbf{v}_n - 4\pi \kappa_{\text{P}} \mathcal{B} + c \kappa_{\text{E}} \mathcal{E} + \Gamma_{\text{diff}}, \quad (1m)$$

<sup>1</sup> We have varied the density  $n_{\text{opq}}$  at which we turn on the radiative transfer solver from  $10^6 - 10^{11} \text{ cm}^{-3}$  and found that  $n_{\text{opq}} \lesssim 10^7 \text{ cm}^{-3}$  is necessary to achieve a smooth transition from isothermality. This numerical necessity does *not* mean that the isothermality assumption breaks down at as low a density as  $10^7 \text{ cm}^{-3}$ .

$$\frac{\partial \mathcal{E}}{\partial t} + \nabla \cdot (\mathcal{E} \mathbf{v}_n) = -\nabla \cdot \mathcal{F} - \nabla \mathbf{v}_n : \mathbf{P} + 4\pi \kappa_P \mathcal{B} - c \kappa_E \mathcal{E}, \quad (1n)$$

$$\frac{\partial \mathcal{F}}{\partial t} + \nabla \cdot (\mathcal{F} \mathbf{v}_n) = -c^2 \nabla \cdot \mathbf{P} - c \chi_{\mathcal{F}} \mathcal{F}. \quad (1o)$$

The quantities  $\rho_s$ ,  $n_s$ , and  $\mathbf{v}_s$  refer to the mass density, number density, and velocity of species  $s$ ; the subscripts n, i, e, g<sub>-</sub>, g<sub>+</sub>, and g<sub>0</sub> refer, respectively, to the neutrals, ions, electrons, negatively-charged grains, positively-charged grains, and neutral grains. The quantities  $\mathbf{E}$  and  $\mathbf{B}$  denote the electric and magnetic field, respectively,  $\mathbf{j}$  the total electric current density,  $u_n$  the internal energy density,  $P_n$  the gas pressure, and  $\psi$  the gravitational potential. The source term  $\Gamma_{\text{diff}}$  in the internal energy equation (1m) represents heating due to ambipolar diffusion and Ohmic dissipation (see § 5.5 below). The magnetic field satisfies the condition  $\nabla \cdot \mathbf{B} = 0$  everywhere at all times. The definitions and derivations of  $\mathbf{F}_{\text{sn}}$  (the frictional force per unit volume on species  $s$  due to elastic collisions with neutrals) and  $\mathbf{F}_{\gamma\delta, \text{inel}}$  (the force per unit volume on grain fluid  $\gamma$  due to the conversion of dust particles of fluid  $\delta$  into dust particles of fluid  $\gamma$ ) are discussed in detail in § 3 of Tassis & Mouschovias (2005a), as well as in Ciolek & Mouschovias (1993) and Mouschovias (1996) (in the absence of positively-charged grains).

The radiation variables are the Planck function  $\mathcal{B}$ , the total (frequency-integrated) radiation energy density  $\mathcal{E}$ , the total (frequency-integrated) radiation momentum density  $\mathcal{F}$ , and the total (frequency-integrated) radiation pressure tensor  $\mathbf{P}$ :

$$\mathcal{E}(\mathbf{x}, t) = \frac{1}{c} \int_0^\infty d\nu \oint d\Omega I(\mathbf{x}, t; \Omega, \nu), \quad (2a)$$

$$\mathcal{F}(\mathbf{x}, t) = \int_0^\infty d\nu \oint d\Omega I(\mathbf{x}, t; \Omega, \nu) \hat{\mathbf{n}}, \quad (2b)$$

$$\mathbf{P}(\mathbf{x}, t) = \frac{1}{c} \int_0^\infty d\nu \oint d\Omega I(\mathbf{x}, t; \Omega, \nu) \hat{\mathbf{n}} \hat{\mathbf{n}}. \quad (2c)$$

Here we have introduced the frequency  $\nu$ , the extinction coefficient (i.e., opacity)  $\chi(\nu) [\equiv \kappa(\nu) + \sigma(\nu)]$ , where  $\kappa$  is the absorption coefficient and  $\sigma$  the scattering coefficient], and the radiation specific intensity  $I$ . The material properties  $\kappa_P$ ,  $\kappa_E$ , and  $\chi_{\mathcal{F}}$  are the Planck and energy mean absorption coefficients, and the flux-weighted mean opacity, respectively; they are given by

$$\kappa_P \equiv \frac{1}{\mathcal{B}} \int_0^\infty \kappa(\nu) \mathcal{B}(\nu) d\nu, \quad \kappa_E \equiv \frac{1}{\mathcal{E}} \int_0^\infty \kappa(\nu) \mathcal{E}(\nu) d\nu, \quad \chi_{\mathcal{F}} \equiv \frac{1}{\mathcal{F}} \int_0^\infty \chi(\nu) \mathcal{F}(\nu) d\nu. \quad (3a,b,c)$$

Equations (1n) and (1o) are obtained from taking moments of the radiation transport equation

$$\left( \frac{1}{c} \frac{\partial}{\partial t} + \Omega \cdot \nabla \right) I(\mathbf{x}, t; \Omega, \nu) = \chi(\mathbf{x}, t; \Omega, \nu) [S(\mathbf{x}, t; \Omega, \nu) - I(\mathbf{x}, t; \Omega, \nu)] \quad (4)$$

under the assumptions that all the radiation variables are measured in the comoving frame of the fluid (in this frame the material properties are isotropic) and that the material properties are grey (Mihalas & Mihalas 1984).<sup>2</sup> We have taken the source function  $S$  in the transport equation (4) to be given by

$$4\pi S_\nu = \frac{4\pi \kappa_\nu \mathcal{B}_\nu + c \sigma_\nu \mathcal{E}_\nu}{\kappa_\nu + \sigma_\nu}, \quad (5)$$

taking into account both establishment of local thermodynamic equilibrium and coherent isotropic scattering of radiation (Mihalas & Mihalas 1984).

In the force equations for the electrons, ions, and grains, the acceleration terms have been neglected due to the small inertia of these species. The acceleration term for the plasma was included by Mouschovias et al. (1985) and it was shown that the plasma reaches a terminal drift velocity very fast. Similarly, the thermal-pressure and gravitational forces have been dropped from the force equations of all species other than the neutrals because they are negligible compared to the electromagnetic and collisional forces. The inelastic momentum transfer by the electron and ion fluids due to attachment onto grains and neutralization are negligible compared to the momentum transfer due to elastic collisions, and they have been omitted from the force equations (1d) and (1e) (see discussion in § 3.1 of Ciolek & Mouschovias 1993). As we consider a distribution of grain sizes, it should be noted that equations (1b), (1f) - (1h) apply to each grain size separately.

The full set of RMHD equations are closed with constitutive relations for the gas pressure, opacities, and the Planck function [i.e.,  $P_n = P_n(\rho_n, T)$ ,  $\chi_{\mathcal{F}} = \chi_{\mathcal{F}}(\rho_g, T)$ ,  $\kappa_E = \kappa_E(\rho_g, T)$ ,  $\kappa_P = \kappa_P(\rho_g, T)$ , and  $\mathcal{B} = \mathcal{B}(T)$ , where  $T$  is the gas temperature and  $\rho_g \equiv \rho_{g-} + \rho_{g_0} + \rho_{g+}$  is the total grain mass density]. In addition, we close the radiation moment equations with the tensor variable Eddington factor  $\mathbf{f}$  which is used to eliminate the radiation stress tensor  $\mathbf{P}$  in favor of the radiation energy density  $\mathcal{E}$  via

$$\mathbf{P} = \mathbf{f} \mathcal{E}. \quad (6)$$

The Eddington factor  $\mathbf{f}$  is determined by employing the flux-limited diffusion approximation (see § 6.1 below). The equation of state for an ideal gas is given by

$$P_n = (\gamma - 1) u_n, \quad (7)$$

<sup>2</sup> We caution here that Preibisch et al. (1995) and Yorke & Sonnhalter (2002) have shown that multi-frequency calculations generally produce higher dust temperatures and greater degrees of anisotropy in the radiation field than corresponding grey calculations.

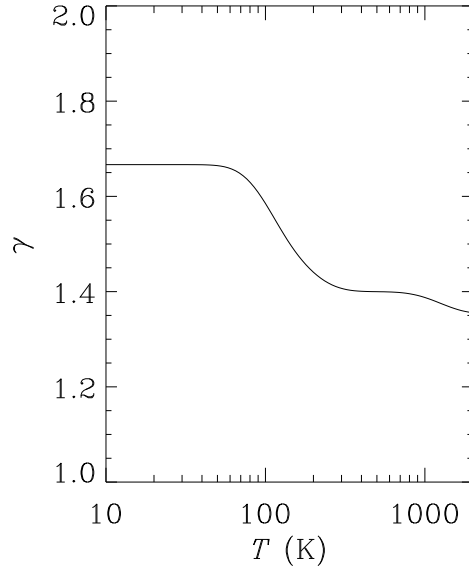


FIG. 1.— Dependence of  $\gamma$  (ratio of specific heats) on temperature for  $\text{H}_2$ .

where  $\gamma = k_B/c_V + 1$  is the adiabatic index and  $c_V$  is the specific heat at constant volume per particle:

$$c_V = \frac{3}{2}k_B + c_V^{\text{vib}} + c_V^{\text{rot}}, \quad (8)$$

assuming that there is no coupling between the rotational and vibrational degrees of freedom of the molecule (in this case,  $\text{H}_2$ ). The vibrational specific heat is

$$c_V^{\text{vib}} = k_B \left( \frac{\Theta_{\text{vib}}}{T} \right)^2 \frac{\exp(\Theta_{\text{vib}}/T)}{[\exp(\Theta_{\text{vib}}/T) - 1]^2}, \quad (9)$$

where  $\Theta_{\text{vib}} = 6100$  K; the rotational specific heat for a 3:1 mixture of ortho- and para-hydrogen is

$$c_V^{\text{rot}} = \frac{3}{4}k_B x^2 \frac{\partial^2}{\partial x^2} \ln Z_o + \frac{1}{4}k_B x^2 \frac{\partial^2}{\partial x^2} \ln Z_p, \quad (10)$$

where  $Z_o$  and  $Z_p$  are the ortho- and para-hydrogen partition functions, respectively, given by

$$Z_o = \sum_{\text{odd } j} (2j+1) \exp[-xj(j+1)] \quad \text{and} \quad Z_p = \sum_{\text{even } j} (2j+1) \exp[-xj(j+1)], \quad (11a,b)$$

and  $x \equiv \Theta_{\text{rot}}/T = 85.4 \text{ K}/T$  (Kittel 1958). The dependence of  $\gamma$  on temperature  $T$  is shown in Figure 1.

Altogether, then, we have a system of 17 equations [(1a) - (1o), (6), and (7)], which contain 21 unknowns ( $\rho_n, P_n, u_n, \mathbf{E}, \mathbf{B}, \mathbf{j}, \psi, \mathbf{v}_n, \mathbf{v}_e, \mathbf{v}_i, \mathbf{v}_{g-}, \mathbf{v}_{g+}, \mathbf{v}_{g0}, \rho_e, \rho_i, \rho_{g-}, \rho_{g+}, \rho_{g0}, \mathcal{E}, \mathcal{F}, \mathbf{P}$ ). To close the system, the densities of electrons, ions, and charged grains ( $n_e, n_i, n_{g-}$ , and  $n_{g+}$ ) are calculated from the equilibrium chemical model described below.

#### 4. THE CHEMICAL MODEL

##### 4.1. Ionization Rate

The rate of ionization per unit volume is given by  $\zeta n_{\text{H}_2}$  and is (in principle) due to the following ionization sources: ultraviolet radiation, cosmic rays, radioactivities, and thermal ionization. The presence of molecules in molecular clouds implies low levels of UV radiation, so it is usually neglected. UV radiation was included by Ciolek & Mouschovias (1995) in their numerical simulations of core formation and evolution. They found that UV ionization dominates cosmic-ray ionization for visual extinctions  $A_V \lesssim 10$  and can increase the degree of ionization in the envelope by at least two orders of magnitude (see also McKee 1989). The increase in ionization was found to *speed up* core collapse by approximately 30% because the central gravitational field of a flattened cloud is stronger (i.e., less diluted by the mass of the envelope) when matter in the envelope is held farther away from the forming core. Once dynamical contraction ensues, it was found that UV radiation has little effect on the evolution of central quantities and therefore it is usually neglected. For numerical reasons, however, we add to the electron and ion number densities the second term in equation (4h) of Fielder & Mouschovias (1992) ( $= 467.64 n_{\text{H}_2}^{-2} \text{ cm}^{-3}$ ) so as to maintain a relatively large degree of ionization ( $\sim 10^{-5} - 10^{-6}$ ) (and therefore negligible ambipolar diffusion) in the low-density ( $n_{\text{H}_2} \lesssim 10^3 \text{ cm}^{-3}$ ) cloud envelope. This term qualitatively mimics the effect of cloud envelope penetration by UV photons, and has negligible quantitative effect on the formation and evolution of the core.

Cosmic rays, on the other hand, with typical energies of 100 MeV are able to penetrate deeper into molecular clouds. Umebayashi & Nakano (1980) have investigated the ionization due to a spectrum of cosmic rays at various energies. They found that the cosmic-ray ionization rate was well described by the following relation:

$$\zeta_{\text{CR}} = \zeta_0 \exp(-\Sigma_{\text{H}_2}/96 \text{ g cm}^{-2}), \quad (12)$$

where  $\Sigma_{\text{H}_2}$  is the column density of  $\text{H}_2$  separating the point in question from the exterior of the cloud and  $\zeta_0 = 5 \times 10^{-17} \text{ s}^{-1}$  is the canonical unshielded cosmic-ray ionization rate (Spitzer 1978). Tassis & Mouschovias (2007b) found that, when a typical core's central density exceeds  $\simeq 10^{12} \text{ cm}^{-3}$ , cosmic rays are shielded and an abrupt decrease in ionization occurs.

Once the core is shielded from high-energy cosmic rays, the dominant source of ionization is radioactive decay of  $^{40}\text{K}$  or  $^{26}\text{Al}$ . The isotope  $^{40}\text{K}$  is the most common radionuclide invoked, due to its long half-life of 1.25 Gyr and its ubiquity in nature (0.012% of terrestrial potassium is  $^{40}\text{K}$ ). The density of potassium in the interstellar medium ( $2.70 \times 10^{-7} n_{\text{H}_2}$ ) and the energy of the beta particle emitted as  $^{40}\text{K}$  decays, 1.31 MeV, are used as inputs to calculate the ionization rate (e.g., see Glassgold 1995):  $\zeta_{40} = 2.43 \times 10^{-23} \text{ s}^{-1}$ . Consolmagno & Jokipii (1978) have suggested that  $^{26}\text{Al}$  may have been a much more potent ionizer than  $^{40}\text{K}$ . Performing a similar calculation for  $^{26}\text{Al}$ , one finds  $\zeta_{26} = 1.94 \times 10^{-19} \text{ s}^{-1}$ , with the fraction of aluminum in the isotope  $^{26}\text{Al}$  inferred to have existed in the solar nebula being  $5 \times 10^{-5}$  (Clayton & Leising 1987). Although  $^{26}\text{Al}$  is four orders of magnitude more potent an ionizer than  $^{40}\text{K}$ , its short half-life (0.716 Myr) makes it relevant only if the initial mass-to-flux ratio of the parent cloud is close to critical, so that the evolution is rapid enough to retain an adequate amount of this radionuclide.  $^{26}\text{Al}$  can also become important if the core happens to get enriched because of a nearby Supernova explosion.

Finally, at temperatures on the order of 1000 K or higher, collisions between molecules are energetic enough to ionize those atoms with low ionization potentials, of which potassium and sodium are the most abundant. The abundance of sodium in the interstellar medium is greater than that of potassium (by a factor  $\simeq 14$ ; Lequeux 1975), but the lower threshold of potassium (4.34 eV vs. 5.13 eV for sodium) makes it the dominant ion. The ionization occurs at a rate (Pneuman & Mitchell 1965) given by

$$\frac{d}{dt}(n_{\text{K}^+}) = 4.1 \times 10^{-15} n_{\text{H}_2} n_{\text{K}^0} \left( \frac{T}{1000 \text{ K}} \right)^{1/2} \exp\left(-\frac{5.04 \times 10^4 \text{ K}}{T}\right) \text{ cm}^3 \text{ s}^{-1}. \quad (13)$$

Because this process relies on collisions between two species, it is not expressed in terms of a quantity  $\zeta$ .

#### 4.2. Grain Size Distribution

Since the dust opacity, the conductivity of the gas, and the collision rates (see below) all depend on the (local) grain surface area, it is necessary to investigate the effect of a grain size distribution. The initial size distributions adopted here are a uniform distribution and the standard "MRN" distribution of interstellar dust (Mathis et al. 1977). In both cases, the density of the solid material of each grain is taken to be  $\rho_{\text{S}} = 2.3 \text{ g cm}^{-3}$ , the average density of silicates. For the uniform distribution, a fiducial grain size  $a_0 = 0.0375 \mu\text{m}$  is used and the total mass density of dust  $\rho_{\text{g,tot}} = 0.01 \rho_{\text{n,tot}}$ . For the MRN distribution, the number density of spherical dust grains with radii between  $a$  and  $a + da$  is

$$dn_{\text{g,tot}}(a) = N_{\text{MRN}} a^{-3.5} da. \quad (14)$$

The distribution is truncated at a lower grain radius  $a_{\text{min}}$  and an upper grain radius  $a_{\text{max}}$ . The coefficient  $N_{\text{MRN}}$  is proportional to the dust-to-gas mass ratio in the cloud. Note that most of the grain surface area is contributed by small grains, because of their overwhelming abundance.

The grains are binned according to size and charge and treated as separate grain species. Each size bin represents a subset of the original distribution of grains, those with radii between  $a_{\text{lower}}$  and  $a_{\text{upper}}$ . The subset of grains in the  $\alpha$ th ( $\alpha = 1, 2, \dots, N$ ) size bin is replaced by a number density  $n_{\text{g}}^{\alpha}$  of grains with identical radii,  $a_{\alpha}$ . The total number of grains and the total surface area of grains in the size bin are constrained to match the total number and surface area of original grains incorporated into the size bin. Hence

$$n_{\text{g}}^{\alpha} = \int_{a_{\text{lower}}}^{a_{\text{upper}}} \frac{dn_{\text{g,tot}}}{da} da, \quad n_{\text{g}}^{\alpha} a_{\alpha}^2 = \int_{a_{\text{lower}}}^{a_{\text{upper}}} a^2 \frac{dn_{\text{g,tot}}}{da} da. \quad (15a,b)$$

Applying these relations to the MRN grain size distribution, equation (14), if there are  $N$  size bins, then the  $\alpha$ th bin is characterized by grains of number density and radii as follows:

$$n_{\text{g}}^{\alpha} = n_{\text{g,tot}} \xi^{2.5(\alpha-1)/N} \left( \frac{1 - \xi^{2.5/N}}{1 - \xi^{2.5}} \right), \quad a_{\alpha} = a_{\text{min}} \xi^{-(\alpha-1)/N} \left[ 5 \left( \frac{1 - \xi^{0.5/N}}{1 - \xi^{2.5/N}} \right) \right]^{1/2}. \quad (16a,b)$$

The ratio of the lower and upper radii of the distribution is denoted by  $\xi \equiv a_{\text{min}}/a_{\text{max}}$ . The total number density of dust,  $n_{\text{g,tot}}$ , is determined by constraining the total grain mass density in the size distribution to be  $\rho_{\text{g,tot}}$ :

$$n_{\text{g,tot}} = \left( \frac{\rho_{\text{g,tot}}}{\frac{4}{3}\pi\rho_{\text{S}}a_{\text{min}}^3} \right) \left[ \frac{1}{5} \left( \frac{1 - \xi^{2.5}}{1 - \xi^{0.5}} \right) \right] \xi^{0.5}. \quad (17)$$

The lower and upper cutoffs to the size distribution are chosen to be  $a_{\text{min}} = 0.0181 \mu\text{m}$  and  $a_{\text{max}} = 0.9049 \mu\text{m}$ , respectively. In equation (17), the total mass density of dust in the system,  $\rho_{\text{g,tot}}$ , is chosen in such a way that the total grain surface area in the size distribution is equal to that in the fiducial case of a single grain size  $a_0$ . This constraint demands that  $\rho_{\text{g,tot}}$  be increased by a factor  $(a_{\text{min}}/a_0) \xi^{-0.5}$  over the fiducial value of  $\rho_{\text{g,tot}}$ . Only in this way can the effect of a size distribution, as distinct from just the surface area of grains, be determined. With the fiducial values  $a_0 = 0.0375 \mu\text{m}$  and  $\rho_{\text{g,tot}} = 0.01 \rho_{\text{n,tot}}$  for the single grain case,  $\rho_{\text{g,tot}} = 0.0341 \rho_{\text{n,tot}}$  for the case of a size distribution. Empirically, it was found that a minimum of five size bins of grain radii were required for convergence of 1%. Since each size grain can be found in one of three possible charge states ( $-e$ ,  $0$ , and  $+e$ ), a total of fifteen grain species are considered.

While we do not consider grain growth (and therefore fix the number of grains within each size bin), we do expect the grain size distribution to evolve spatially within the star-forming cloud. Ambipolar diffusion can alter a grain size distribution by acting

more effectively on the larger grains, causing a spatial segregation of grain sizes that leaves the smaller grains behind in the cloud envelope. The result is a deficit of small grains ( $a \lesssim 10^{-5}$  cm) in the cloud core. In fact, Ciolek & Mouschovias (1996) show how observations of grain abundances in the core and envelope of a molecular cloud can, at least in principle, be used to determine the initial mass-to-flux ratio of the cloud.

### 4.3. Chemical Network

We use a chemical equilibrium network accounting for electrons (subscript e); molecular ions such as  $\text{HCO}^+$  (subscript  $m^+$ ); neutral metal atoms (subscript  $A^0$ ) and atomic ions (subscript  $A^+$ ) of Mg, Na, and K; singly positively-charged grains (subscript  $g_+$ ); singly negatively-charged grains (subscript  $g_-$ ); and, neutral grains (subscript  $g_0$ ). Multiply negatively- (positively-)charged grains may be neglected, because a singly negatively- (positively-)charged grain repels electrons (ions) thereby decreasing the rate of capture by the factor  $\exp(-e^2/ak_B T)$  (Spitzer 1941). The equilibrium assumption is accurate provided that the dynamical timescales of interest are sufficiently longer than the chemical-reaction timescales. This is always the case for the density regime considered here. The relevant reactions are given below and explained briefly.

The production of molecular ions (such as  $\text{HCO}^+$ ) is balanced by their destruction through charge-exchange reactions with atomic ions, by dissociative recombinations (collisions with electrons), or by collisions with and neutralization on the surfaces of grains:

$$\zeta n_{\text{H}_2} = n_{m^+} n_{A^0} \beta + n_{m^+} n_e \alpha_{\text{dr}} + \sum_{\alpha} n_{m^+} n_{g_-^{\alpha}} \alpha_{m^+ g_-^{\alpha}} + \sum_{\alpha} n_{m^+} n_{g_0^{\alpha}} \alpha_{m^+ g_0^{\alpha}}. \quad (18)$$

The index  $\alpha$  denotes a grain size bin, and the sum is over all the size bins, which are treated as independent grain species. The production of atomic ions by charge-exchange reactions is balanced by radiative recombinations and by collisions with grains:

$$n_{m^+} n_{A^0} \beta = n_{A^+} n_e \alpha_{\text{rr}} + \sum_{\alpha} n_{A^+} n_{g_-^{\alpha}} \alpha_{A^+ g_-^{\alpha}} + \sum_{\alpha} n_{A^+} n_{g_0^{\alpha}} \alpha_{A^+ g_0^{\alpha}}. \quad (19)$$

If the atomic ion in question is  $\text{K}^+$ , there is the additional source term due to thermal ionization of potassium atoms,  $n_{\text{K}^0} n_{\text{H}_2} \alpha_{\text{K}^0 \text{H}_2}$ . Positively-charged grains are formed by the collisions of ions and neutral grains and by charge exchange between grains; they are destroyed by collisions with electrons, collisions with negative grains, and by charge exchange with neutral grains:

$$n_{m^+} n_{g_0^{\alpha}} \alpha_{m^+ g_0^{\alpha}} + n_{A^+} n_{g_0^{\alpha}} \alpha_{A^+ g_0^{\alpha}} + \sum_{\alpha'} n_{g_+^{\alpha'}} n_{g_0^{\alpha}} \alpha_{g_+^{\alpha'} g_0^{\alpha}} = n_e n_{g_+^{\alpha}} \alpha_{e g_+^{\alpha}} + \sum_{\alpha'} n_{g_+^{\alpha}} n_{g_-^{\alpha'}} \alpha_{g_+^{\alpha} g_-^{\alpha'}} + \sum_{\alpha'} n_{g_+^{\alpha}} n_{g_0^{\alpha'}} \alpha_{g_+^{\alpha} g_0^{\alpha'}}. \quad (20)$$

Here the index  $\alpha'$  runs over all the grain size bins, independently of the index  $\alpha$ . Negatively-charged grains are formed by the collisions of electrons and neutral grains and by charge exchange between grains, and are destroyed by collisions with ions, collisions with positive grains, and by charge exchange with neutral grains:

$$n_e n_{g_0^{\alpha}} \alpha_{e g_0^{\alpha}} + \sum_{\alpha'} n_{g_-^{\alpha'}} n_{g_0^{\alpha}} \alpha_{g_-^{\alpha'} g_0^{\alpha}} = n_{m^+} n_{g_-^{\alpha}} \alpha_{m^+ g_-^{\alpha}} + n_{A^+} n_{g_-^{\alpha}} \alpha_{A^+ g_-^{\alpha}} + \sum_{\alpha'} n_{g_+^{\alpha'}} n_{g_-^{\alpha}} \alpha_{g_+^{\alpha'} g_-^{\alpha}} + \sum_{\alpha'} n_{g_-^{\alpha}} n_{g_0^{\alpha'}} \alpha_{g_-^{\alpha} g_0^{\alpha'}}. \quad (21)$$

We close this set of equations with constraints on the total number of grains in a given size bin,

$$n_{g_+^{\alpha}} + n_{g_0^{\alpha}} + n_{g_-^{\alpha}} = n_{g^{\alpha}}, \quad (22)$$

and the total number of an atomic species (neutral + positively-charged),

$$n_{A^0} + n_{A^+} = n_A, \quad (23)$$

and with charge neutrality:

$$n_{m^+} + n_{A^+} - n_e + \sum_{\alpha} (n_{g_+^{\alpha}} - n_{g_-^{\alpha}}) = 0. \quad (24)$$

This system of equations [(18) - (24)] is solved numerically via Gauss-Jordan elimination on the matrix equation derived by applying the Newton-Raphson iteration method. The rate coefficients in equations (18) - (24) are given in Appendix A.

The mass of molecular ions is taken to be that of  $\text{HCO}^+$ ,  $m_{m^+} = 29 m_p$ , while for the atomic ions an average value  $m_{A^+} = 23.5 m_p$ , between the mass of Na ( $m_{\text{Na}^+} = 23 m_p$ ) and the mass of Mg ( $m_{\text{Mg}^+} = 24 m_p$ ), is used. Since the ion masses are all comparable, the fact that different ionic species dominate in different density regimes does not affect the evolution of the cloud cores. The total number of atomic ions is fixed at  $2.05 \times 10^{-6} n_n$  (Morton 1974; Snow 1976).

## 5. MAGNETIC FLUX LOSS AND ELECTRICAL RESISTIVITY

The force equations [(1d) - (1h)] and the induction equation (1k) are not written in the most convenient form for our purposes (see § 7 below). A useful simplification can be made, which amounts to a generalized version of Ohm's law; namely, we replace equations (1d) - (1h) with a modified form of equation (1k). This auspiciously eliminates 5 variables ( $\mathbf{v}_e$ ,  $\mathbf{v}_i$ ,  $\mathbf{v}_{g_0}$ ,  $\mathbf{v}_{g_-}$ , and  $\mathbf{v}_{g_+}$ ), but not without a cost. The ensuing algebra is messy, and much of it is deferred to Appendix B.1. Here, we outline the simplification and highlight some results suitable for the present discussion.



### 5.1. Resistivity of a Magnetic Gas

The rate of change of magnetic flux across a given surface  $S$ , comoving with a fluid with velocity  $\mathbf{v}$ , is given by

$$\frac{d\Phi_B}{dt} = \int_S \left[ \frac{\partial \mathbf{B}}{\partial t} - \nabla \times (\mathbf{v} \times \mathbf{B}) \right] \cdot d\mathbf{S}. \quad (25)$$

Using Faraday's law (1k), the integrand can be rewritten as

$$\frac{d\Phi_B}{dt} = -c \int_S \nabla \times \left( \mathbf{E} + \frac{\mathbf{v}}{c} \times \mathbf{B} \right) \cdot d\mathbf{S}, \quad (26)$$

and the current density can be calculated from

$$\mathbf{j} = \boldsymbol{\sigma} \left( \mathbf{E} + \frac{\mathbf{v}}{c} \times \mathbf{B} \right). \quad (27)$$

The quantity  $\mathbf{v}$  is the velocity of the fluid, which for a weakly-ionized gas is essentially that of the neutrals  $\mathbf{v}_n$ , and  $\boldsymbol{\sigma}$  is the conductivity tensor. The presence of a magnetic field introduces an anisotropy in the equations, which is the reason for which the conductivity must be described by a tensor. If we take the 3-direction to lie along the magnetic field, the conductivity tensor has the following representation (Parks 1991):

$$\boldsymbol{\sigma} = \begin{pmatrix} \sigma_{\perp} & -\sigma_H & 0 \\ \sigma_H & \sigma_{\perp} & 0 \\ 0 & 0 & \sigma_{\parallel} \end{pmatrix}. \quad (28)$$

As  $B \rightarrow 0$ , the tensor must reduce to an isotropic form; i.e.,  $\sigma_H \rightarrow 0$  and  $\sigma_{\perp} \rightarrow \sigma_{\parallel}$ . Because magnetic forces vanish along the magnetic field,  $\sigma_{\parallel}$  must be independent of the magnetic field strength.

Equation (27) may be inverted to obtain the electric field, in which case a resistivity tensor  $\boldsymbol{\eta}$  is defined by

$$\mathbf{E} + \frac{\mathbf{v}_n}{c} \times \mathbf{B} = \boldsymbol{\eta} \mathbf{j}, \quad (29)$$

where, in the same representation as  $\boldsymbol{\sigma}$  written above,

$$\boldsymbol{\eta} = \begin{pmatrix} \eta_{\perp} & \eta_H & 0 \\ -\eta_H & \eta_{\perp} & 0 \\ 0 & 0 & \eta_{\parallel} \end{pmatrix}, \quad (30)$$

and

$$\eta_{\parallel} = \frac{1}{\sigma_{\parallel}}, \quad \eta_{\perp} = \frac{\sigma_{\perp}}{\sigma_{\perp}^2 + \sigma_H^2}, \quad \eta_H = \frac{\sigma_H}{\sigma_{\perp}^2 + \sigma_H^2}. \quad (31a,b,c)$$

The flux-freezing approximation corresponds to the limit  $\boldsymbol{\eta} \rightarrow 0$ .

If we write the current density  $\mathbf{j}$  in component form, it follows that we may write equation (29) as

$$\mathbf{E} + \frac{\mathbf{v}_n}{c} \times \mathbf{B} = \eta_{\parallel} \mathbf{j}_{\parallel} + \eta_{\perp} \mathbf{j}_{\perp} + \eta_H \mathbf{j} \times \mathbf{b}, \quad (32)$$

where  $\mathbf{j}_{\parallel}$  and  $\mathbf{j}_{\perp}$  are the components of the current density parallel and perpendicular to the magnetic field, respectively, and  $\mathbf{b}$  is a unit vector along the magnetic field. This relation between the electric field and the current density can be substituted in equation (26) to find that

$$\frac{d\Phi_B}{dt} = -c \int_S \nabla \times (\eta_{\parallel} \mathbf{j}_{\parallel} + \eta_{\perp} \mathbf{j}_{\perp} + \eta_H \mathbf{j} \times \mathbf{b}) \cdot d\mathbf{S}. \quad (33)$$

This is the general form of the equation describing the loss of magnetic flux from a parcel of neutral gas, written entirely in terms of the components of the resistivity and current density tensors.

For our model cloud, we have assumed axisymmetry and neglected rotation. In this case, the magnetic field is purely poloidal and the current density is purely toroidal by Ampere's law (1i). This geometry implies that the only nonvanishing component of the current density is the component perpendicular to the magnetic field,  $\mathbf{j} = \mathbf{j}_{\perp}$ . The evolution of the poloidal magnetic flux in the neutrals' reference frame is then given by

$$\frac{d\Phi_B}{dt} = -c \int_S \nabla \times (\eta_{\perp} \mathbf{j}_{\perp}) \cdot d\mathbf{S}. \quad (34)$$

The equivalent equation governing the evolution of the poloidal magnetic field is

$$\frac{\partial \mathbf{B}}{\partial t} = \nabla \times (\mathbf{v}_n \times \mathbf{B}) - c \nabla \times (\eta_{\perp} \mathbf{j}_{\perp}). \quad (35)$$

Equation (34) describes the evolution of magnetic flux in the neutrals' reference frame due to the motion of charges at right angles to the magnetic field and includes the effects of both ambipolar diffusion and Ohmic dissipation. The rate at which magnetic flux is lost equals the sum of the rates due to each process. Therefore,  $\eta_{\perp}$  can itself be written as the sum of two components, one related to ambipolar diffusion (subscript AD) and the other to Ohmic dissipation (subscript OD):

$$\eta_{\perp} = \eta_{\perp AD} + \eta_{\perp OD}. \quad (36)$$

The issue of how to separate the resistivity  $\eta_{\perp}$  into its two components is discussed, for example, in Nakano & Umebayashi (1986a,b), Goldreich & Reisenegger (1992), and Desch & Mouschovias (2001). We quote the result here:

$$\eta_{\parallel OD} = \eta_{\parallel}, \quad \eta_{\perp OD} = \eta_{\perp}, \quad \eta_{\parallel AD} = 0, \quad \eta_{\perp AD} = \eta_{\perp} - \eta_{\parallel}. \quad (37a,b,c,d)$$

We now derive expressions for the resistivities from first principles.

### 5.2. Generalized Ohm's Law

We outline the derivation of a generalized Ohm's law, taking into account both elastic and inelastic collisions between neutrals, ions, electrons, and charged and neutral grains. We begin by writing down the force equation for the charged species  $s$ :

$$0 = n_s q_s \left( \mathbf{E} + \frac{\mathbf{v}_s}{c} \times \mathbf{B} \right) + \frac{\rho_s}{\tau_{sn}} (\mathbf{v}_n - \mathbf{v}_s) + \frac{\rho_{g_0}}{\tau_{s,\text{inel}}} (\mathbf{v}_{g_0} - \mathbf{v}_s). \quad (38)$$

The subscript  $s$  runs over all the charged species, taking on the values  $s = i, e, g_+,$  and  $g_-$ . Although we employ a grain size distribution, we consider only a single grain size in what follows for ease of presentation; a discussion of the consequences of a grain size distribution is deferred to Appendix B.2. The charge  $q_s$  of species  $s$  carries an algebraic sign (e.g., it is negative for electrons). We write  $\tau_{s,\text{inel}}$  to represent the timescale for species  $s$  to be created by or take part in any inelastic collision. For example,

$$\tau_{g_+,\text{inel}} = \left[ \frac{1}{\tau_{g_0 i,\text{inel}}} + \frac{1}{\tau_{g_0 g_+,\text{inel}}} + \frac{\rho_{g_+}}{\rho_{g_0}} \left( \frac{1}{\tau_{g_+ e,\text{inel}}} + \frac{1}{\tau_{g_+ g_-,\text{inel}}} + \frac{1}{\tau_{g_+ g_0,\text{inel}}} \right) \right]^{-1} \quad (39)$$

is the timescale for a neutral grain to participate in *any* inelastic reaction involving conversion between positive and neutral grains. The first two terms represent the production of positive grains due to charge exchange between neutral grains and ions and between neutral grains and positive grains, respectively; the next two terms represent the conversion of positive grains to neutral grains via neutralization with electrons and negative grains, respectively; and, the final term represents the conversion of positive grains to neutral grains via charge exchange. Since these are processes occurring in parallel, the reciprocals of their respective collision times are added to obtain the net collision time. Similarly,

$$\tau_{g_-,\text{inel}} = \left[ \frac{1}{\tau_{g_0 e,\text{inel}}} + \frac{1}{\tau_{g_0 g_-,\text{inel}}} + \frac{\rho_{g_-}}{\rho_{g_0}} \left( \frac{1}{\tau_{g_- i,\text{inel}}} + \frac{1}{\tau_{g_- g_+,\text{inel}}} + \frac{1}{\tau_{g_- g_0,\text{inel}}} \right) \right]^{-1} \quad (40)$$

is the timescale for a neutral grain to be involved in *any* inelastic reaction involving conversion between negative and neutral grains. The force equation for the neutral grains is

$$0 = \frac{\rho_{g_0}}{\tau_{g_0 n}} (\mathbf{v}_n - \mathbf{v}_{g_0}) + \sum_k \frac{\rho_{g_0}}{\tau_{k,\text{inel}}} (\mathbf{v}_k - \mathbf{v}_{g_0}), \quad (41)$$

where the index  $k$  runs over all the charged species.

We eliminate the velocity  $\mathbf{v}_s$  of species  $s$  in favor of a new velocity,  $\mathbf{w}_s$ , which is the velocity of species  $s$  with respect to the neutral gas ( $\mathbf{w}_s \equiv \mathbf{v}_s - \mathbf{v}_n$ ). In addition, we define  $\mathbf{E}_n$  as the electric field in the frame of reference of the neutral gas ( $\mathbf{E}_n \equiv \mathbf{E} + \mathbf{v}_n \times \mathbf{B}/c$ ). Equations (38) and (41) then become, respectively,

$$0 = \frac{\omega_s \tau_{sn}}{1 + \varrho_s} \left( \frac{c}{B} \mathbf{E}_n + \mathbf{w}_s \times \mathbf{b} \right) - \mathbf{w}_s + \frac{\varrho_s}{1 + \varrho_s} \mathbf{w}_{g_0}, \quad (42)$$

$$0 = \mathbf{w}_{g_0} - \sum_k \frac{\tau_0}{\tau_{k,\text{inel}}} \mathbf{w}_k, \quad (43)$$

where we have introduced the cyclotron frequency of species  $s$ ,  $\omega_s = q_s B / m_s c$ , and have defined  $\varrho_s$  and  $\tau_0$  by

$$\varrho_s = \frac{\rho_{g_0}}{\rho_s} \frac{\tau_{sn}}{\tau_{s,\text{inel}}} \quad \text{and} \quad \frac{1}{\tau_0} = \frac{1}{\tau_{g_0 n}} + \sum_k \frac{1}{\tau_{k,\text{inel}}}. \quad (44a,b)$$

Equations (42) and (43) form the set of equations to be solved.<sup>3</sup> The species velocities (relative to the neutrals)  $\mathbf{w}_s$  can be expressed in terms of  $\mathbf{E}_n$  and then substituted in the definition of the current density

$$\mathbf{j} = \sum_s n_s q_s \mathbf{w}_s, \quad (45)$$

where we have used charge neutrality ( $\sum_s n_s q_s = 0$ ). This expression can then be inverted to find  $\mathbf{E}_n$  in terms of  $\mathbf{j}$ , which defines the resistivity tensor. The magnetic induction equation is then found by substitution into Faraday's law of induction:

$$\frac{\partial \mathbf{B}}{\partial t} - \nabla \times (\mathbf{v}_n \times \mathbf{B}) = -c \nabla \times \mathbf{E}_n. \quad (46)$$

Using this approach, we derive an induction equation generalized to include Ohmic dissipation, ambipolar diffusion, and the Hall effect for a six-fluid system including both elastic and inelastic collisions.

The ensuing calculation is tedious, and we defer the details to Appendix B.1. Here we give only the final result:

$$\mathbf{j} = \sigma_{||} \mathbf{E}_{n,||} + \sigma_{\perp} \mathbf{E}_{n,\perp} - \sigma_H \mathbf{E}_n \times \mathbf{b}, \quad (47)$$

where

$$\sigma_{||} = \sum_s \sigma_s (1 - \varsigma_s), \quad \sigma_{\perp} = \sum_s \frac{\sigma_s (1 - \varsigma_s)}{1 + \omega_s^2 \tau_{sn}^2 (1 - \varphi_s)} \Upsilon_s(\varsigma), \quad \sigma_H = - \sum_s \frac{\sigma_s \omega_s \tau_{sn} (1 - \varpi_s)}{1 + \omega_s^2 \tau_{sn}^2 (1 - \varphi_s)} \Upsilon_s(\varpi). \quad (48a,b,c)$$

<sup>3</sup> The quantity  $\varrho_s$  was written as  $r_s$  in Tassis & Mouschovias (2007a). We have renamed it here to avoid confusion with the cylindrical radial coordinate  $r$ .

The conductivity of species  $s$  is given by  $\sigma_s = n_s q_s^2 \tau_{sn} / m_s$ . The quantities  $\zeta_s$ ,  $\varpi_s$ ,  $\varphi_s$ , and  $\Upsilon_s$  are defined in Appendix D; they represent the effects of inelastic collisions on the conductivity of the gas. In the absence of inelastic collisions, these formulae reduce to their standard form (e.g., see Parks 1991):

$$\sigma_{||} \rightarrow \sum_s \sigma_s, \quad \sigma_{\perp} \rightarrow \sum_s \frac{\sigma_s}{1 + \omega_s^2 \tau_{sn}^2}, \quad \sigma_H \rightarrow - \sum_s \frac{\sigma_s \omega_s \tau_{sn}}{1 + \omega_s^2 \tau_{sn}^2}.$$

Equation (47) may be inverted to give

$$\mathbf{E}_n = \eta_{||} \mathbf{j}_{||} + \eta_{\perp} \mathbf{j}_{\perp} + \eta_H \mathbf{j} \times \mathbf{b}, \quad (49)$$

with the resistivities  $\eta_{||}$ ,  $\eta_{\perp}$ , and  $\eta_H$  given by equations (31).

### 5.3. Attachment of Species to Magnetic Field Lines

It is possible to write the velocity of each species,  $\mathbf{v}_s$ , in terms of the velocity of the neutrals,  $\mathbf{v}_n$ , and the velocity of the field lines,  $\mathbf{v}_f$ , which is defined implicitly by

$$\mathbf{E} + \frac{\mathbf{v}_f}{c} \times \mathbf{B} = 0. \quad (50)$$

The algebra and some intermediate results of interest are given in Appendix C; here, we quote the main result and explain it physically:

$$\mathbf{v}_{s,\perp} = \mathbf{v}_{n,\perp} \frac{1}{\Theta_s + 1} + \mathbf{v}_{f,\perp} \frac{\Theta_s}{\Theta_s + 1} + (\mathbf{v}_f - \mathbf{v}_n) \times \mathbf{b} \Lambda_s, \quad (51a)$$

$$\mathbf{v}_s \times \mathbf{b} = \mathbf{v}_n \times \mathbf{b} \frac{1}{\Theta_s + 1} + \mathbf{v}_f \times \mathbf{b} \frac{\Theta_s}{\Theta_s + 1} - (\mathbf{v}_{f,\perp} - \mathbf{v}_{n,\perp}) \Lambda_s, \quad (51b)$$

where the expressions for  $\Theta_s$  and  $\Lambda_s$  are given in Appendix C. The quantity  $\Theta_s$  is the *attachment parameter* (i.e., for  $\Theta_s \gg 1$ ,  $\mathbf{v}_s \approx \mathbf{v}_f$  and species  $s$  is attached to the field lines, whereas for  $\Theta_s \ll 1$ ,  $\mathbf{v}_s \approx \mathbf{v}_n$  and species  $s$  is detached and comoves with the neutrals) — see, also, Ciolek & Mouschovias (1993), § 3.1.2. The function  $\Lambda_s$  quantifies the relation of one component of the species velocity to its mutually perpendicular component of the field line drift velocity, and essentially embodies Ampere's law. Under the assumptions of this paper, the midplane velocities of the charged species  $s$ , written in cylindrical coordinates  $(r, \phi, z)$ , are

$$\mathbf{v}_{s,\phi}(r, z = 0) = (\mathbf{v}_{n,r} - \mathbf{v}_{f,r}) \Lambda_s, \quad \mathbf{v}_{s,r}(r, z = 0) = \mathbf{v}_{n,r} \frac{1}{\Theta_s + 1} + \mathbf{v}_{f,r} \frac{\Theta_s}{\Theta_s + 1}. \quad (52a,b)$$

The first equation says that the charged species move in such a way as to cause differential motion between the field lines and the neutrals (Ampere's law). The second equation gives the radial velocity of any charged species in terms of the the velocities of the neutrals and of the field lines. These may be combined to yield

$$\mathbf{w}_{s,r} = \mathbf{v}_{s,r} - \mathbf{v}_{n,r} = - \frac{\Theta_s}{\Theta_s + 1} \frac{\mathbf{v}_{s,\phi}}{\Lambda_s}. \quad (53)$$

In other words, the radial drift between species  $s$  and the neutrals is directly proportional to the contribution of species  $s$  to the azimuthal current.

### 5.4. Grain Continuity Equation

In the notation of Section 5.2, the grain continuity equation (1b) may be written as

$$\frac{\partial \rho_g}{\partial t} + \nabla \cdot (\rho_g \mathbf{v}_n) = - \nabla \cdot (\rho_{g-} \mathbf{w}_{g-} + \rho_{g0} \mathbf{w}_{g0} + \rho_{g+} \mathbf{w}_{g+}), \quad (54)$$

where  $\rho_g = \rho_{g-} + \rho_{g0} + \rho_{g+}$  is the total grain density. Eliminating  $\mathbf{w}_{g0}$  using equation (43), we find that

$$\frac{\partial \rho_g}{\partial t} + \nabla \cdot (\rho_g \mathbf{v}_n) = - \nabla \cdot \left[ \rho_{g+} \mathbf{w}_{g+} \left( 1 + \frac{\tau_0}{\tau_{g+n}} \varrho_{g+} \right) + \rho_{g-} \mathbf{w}_{g-} \left( 1 + \frac{\tau_0}{\tau_{g-n}} \varrho_{g-} \right) \right]. \quad (55)$$

We may use equation (C1) to eliminate the differential velocities of the charged grain species to find, after some manipulation,

$$\frac{\partial \rho_g}{\partial t} + \nabla \cdot (\rho_g \mathbf{v}_n) = - \nabla \cdot (\eta_{\text{cont},||} \mathbf{j}_{||} + \eta_{\text{cont},\perp} \mathbf{j}_{\perp} + \eta_{\text{cont},H} \mathbf{j} \times \mathbf{b}), \quad (56)$$

where the components of the grain-continuity resistivity tensor,  $\eta_{\text{cont}}$ , are defined as

$$\eta_{\text{cont},||} = \sum_{s=g+,g-} \frac{m_s}{q_s} \left[ \eta_{||} \sigma_{||,s} \left( 1 + \frac{\tau_0}{\tau_{sn}} \varrho_s \right) \right], \quad (57a)$$

$$\eta_{\text{cont},\perp} = \sum_{s=g+,g-} \frac{m_s}{q_s} \left[ \eta_{\perp} \sigma_{\perp,s} \left( 1 + \frac{\tau_0}{\tau_{sn}} \varrho_s \right) - \eta_H \sigma_{H,s} \left( 1 + \frac{\tau_0}{\tau_{sn}} \varrho_s \right) \right], \quad (57b)$$

$$\eta_{\text{cont,H}} = \sum_{s=\text{g}^+,\text{g}^-} \frac{m_s}{q_s} \left[ \eta_{\text{H}} \sigma_{\perp,s} \left( 1 + \frac{\tau_0}{\tau_{\text{sn}}} \varrho_s \right) - \eta_{\perp} \sigma_{\text{H},s} \left( 1 + \frac{\tau_0}{\tau_{\text{sn}}} \varrho_s \right) \right]. \quad (57\text{c})$$

These equations apply to all grain sizes separately. Under the assumptions in this work,  $\mathbf{j}_{\parallel} = 0$  and  $\nabla \cdot \mathbf{j}_{\perp} = 0$  by axisymmetry. Equation (56) then becomes

$$\frac{\partial \rho_{\text{g}}}{\partial t} + \nabla \cdot (\rho_{\text{g}} \mathbf{v}_{\text{n}}) = -\nabla \cdot (\eta_{\text{cont,H}} \mathbf{j} \times \mathbf{b}). \quad (58)$$

Note that if  $\eta_{\text{cont,H}} = 0$ , a quantitative implementation of flux-freezing, the grain species are advected with the neutrals, as expected.

### 5.5. Joule Heating

The rate  $\Gamma_{\text{diff}}$  at which collisions dissipate kinetic energy as heat per unit volume (in the reference frame of the neutrals) may be calculated by taking the dot product of equation (42) with  $\mathbf{w}_s$  and using equation (41):

$$\Gamma_{\text{diff}} = \left[ \sum_s (1 + \varrho_s) \frac{\rho_s}{\tau_{\text{sn}}} |\mathbf{w}_s|^2 \right] - \left( \sum_s \frac{\rho_{\text{g}0}}{\tau_{s,\text{inel}}} \mathbf{w}_s \right) \cdot \left( \sum_k \frac{\tau_0}{\tau_{k,\text{inel}}} \mathbf{w}_k \right), \quad (59)$$

where the summation indices  $s$  and  $k$  run, as usual, over all charged species (including charged grains of different sizes if a grain size distribution is considered). Using equation (C1) to eliminate the velocities in favor of the current density, we find after much simplification

$$\begin{aligned} \Gamma_{\text{diff}} = & \eta_{\parallel} |\mathbf{j}_{\parallel}|^2 \left[ \sum_s \left( \frac{\sigma_{\parallel,s}}{\sqrt{\sigma_s \sigma_{\parallel}}} \sqrt{1 + \varrho_s} \right)^2 - \left( \sum_s \frac{\sigma_{\parallel,s}}{\sqrt{\sigma_s \sigma_{\parallel}}} \sqrt{\frac{\varrho_s \tau_0}{\tau_{s,\text{inel}}}} \right)^2 \right] \\ & + \eta_{\perp} |\mathbf{j}_{\perp}|^2 \left[ \sum_s \left( \frac{\sigma_{\perp,s}}{\sqrt{\sigma_s \sigma_{\perp}}} \sqrt{1 + \varrho_s} \right)^2 - \left( \sum_s \frac{\sigma_{\perp,s}}{\sqrt{\sigma_s \sigma_{\perp}}} \sqrt{\frac{\varrho_s \tau_0}{\tau_{s,\text{inel}}}} \right)^2 \right] \\ & + \eta_{\text{H}} |\mathbf{j}_{\perp}|^2 \left[ \sum_s \left( \frac{\sigma_{\text{H},s}}{\sqrt{\sigma_s \sigma_{\text{H}}}} \sqrt{1 + \varrho_s} \right)^2 - \left( \sum_s \frac{\sigma_{\text{H},s}}{\sqrt{\sigma_s \sigma_{\text{H}}}} \sqrt{\frac{\varrho_s \tau_0}{\tau_{s,\text{inel}}}} \right)^2 \right]. \end{aligned} \quad (60)$$

In the limit where inelastic collisions are negligible relative to elastic collisions (i.e.,  $\varrho_s \rightarrow 0$ ), this equation reduces to the usual expression

$$\Gamma_{\text{diff}} \rightarrow \eta_{\parallel} |\mathbf{j}_{\parallel}|^2 + \eta_{\perp} |\mathbf{j}_{\perp}|^2 = \eta_{\text{OD}} |\mathbf{j}|^2 + \eta_{\text{AD}} |\mathbf{j}_{\perp}|^2.$$

In the last step, we have used equations (37) to separate the contributions of Ohmic dissipation and ambipolar diffusion to the heating rate. Ohmic dissipation affects the total current density, whereas ambipolar diffusion affects only the perpendicular component of the current density.

## 6. RADIATIVE TRANSFER

### 6.1. The Flux-Limited Diffusion Approximation

Computing a formal solution of the full angle-frequency dependent non-LTE radiative transfer equation in a multidimensional numerical algorithm is a prohibitive task. Even if a rigorous yet tractable algorithm were developed to this end, the computational expense involved would prevent a solution in any reasonable amount of time. In fact, the sophisticated numerical code described in Stone et al. (1992) designed to solve this problem with as few approximations as possible never saw public release. The FLD approximation is an attractive method for handling transport phenomena that is relatively easy to implement, robust, and inexpensive. It has the advantage over other diffusive approximations in that it preserves causality in regions where significant spatial variation can occur over distances smaller than a mean free path. For example, the Eddington approximation consists of assuming the radiation field is everywhere isotropic, an assumption that is violated in the optically-thin limit where the radiation becomes streaming (Mihalas & Mihalas 1984).

The fundamental assumption of FLD is that the specific intensity is a slowly varying function of space and time. This is certainly valid in the diffusion and streaming limits (at least in one dimension); one hopes that it is approximately true in intermediate situations (and in multi-dimensions). Given this assumption, Levermore & Pomraning (1981) showed that the radiation flux can be expressed in the form of Fick's law of diffusion,

$$\mathcal{F} = -\mathcal{D}_{\text{FLD}} \nabla \mathcal{E}, \quad (61)$$

where the diffusion coefficient  $\mathcal{D}_{\text{FLD}}$  can be written as

$$\mathcal{D}_{\text{FLD}} = \frac{c \lambda_{\text{FLD}}}{\chi_{\mathcal{F}}}. \quad (62)$$

The dimensionless function  $\lambda_{\text{FLD}} = \lambda_{\text{FLD}}(\mathcal{E})$  is called the flux limiter. Similarly, in FLD theory the radiation pressure tensor can be expressed in terms of the radiation energy density via

$$\mathbf{P} = \mathbf{f} \mathcal{E}, \quad (63)$$

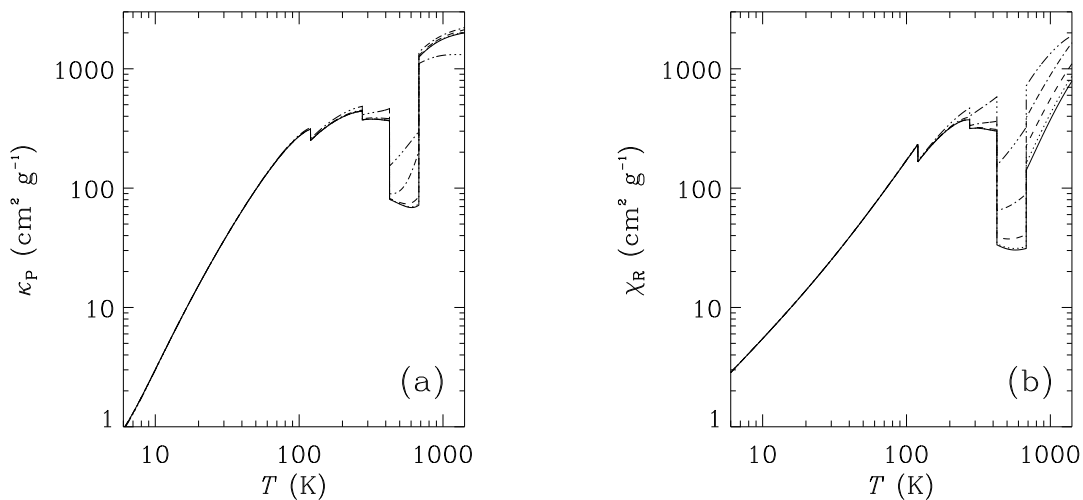


FIG. 2.— (a) Planck mean absorption coefficients and (b) Rosseland mean extinction coefficients (in  $\text{cm}^2$  per gram of dust) for grain sizes  $a = 0.0256 \mu\text{m}$  (solid line),  $0.0543 \mu\text{m}$  (dotted line),  $0.1190 \mu\text{m}$  (dashed line),  $0.2600 \mu\text{m}$  (dash-dot line), and  $0.5680 \mu\text{m}$  (dash-dot-dot-dot line).

where the components of the Eddington tensor  $\mathbf{f}$  are given by

$$\mathbf{f} = \frac{1}{2}(1 - f)\mathbf{I} + \frac{1}{2}(3f - 1)\hat{\mathbf{n}}\hat{\mathbf{n}}, \quad (64)$$

where  $\hat{\mathbf{n}} = \nabla\mathcal{E}/|\nabla\mathcal{E}|$  is the normalized gradient of  $\mathcal{E}$  and the dimensionless function  $f = f(\mathcal{E})$  is called the Eddington factor (Turner & Stone 2001). The flux limiter  $\lambda_{\text{FLD}}$  and Eddington factor  $f$  are related through implicit constraints between the moments  $\mathcal{F}$  and  $\mathbf{P}$ , so that

$$f = \lambda_{\text{FLD}} + \lambda_{\text{FLD}}^2 \mathcal{R}^2, \quad (65)$$

where  $\mathcal{R}$  is the dimensionless quantity  $\mathcal{R} = |\nabla\mathcal{E}|/\chi_{\mathcal{F}}\mathcal{E}$ . We have chosen the flux limiter derived by Levermore & Pomraning (1981, eq. 28), which is given by

$$\lambda_{\text{FLD}} = \frac{2 + \mathcal{R}}{6 + 3\mathcal{R} + \mathcal{R}^2}. \quad (66)$$

Its use in hydrodynamic simulations of star formation has been documented, for example, in Bodenheimer et al. (1990), Bodenheimer et al. (1993, 1995), and Whitehouse & Bate (2006).

## 6.2. Dust Opacities

For temperature less than  $\simeq 1500$  K, the contribution of dust to the total opacity dominates that from all other sources. We take  $\kappa_{\text{E}} = \kappa_{\text{P}}$  and  $\chi_{\mathcal{F}} = \chi_{\text{R}}$  (see Mihalas & Mihalas 1984, § 82), where  $\kappa_{\text{P}}$  and  $\chi_{\text{R}}$  have been obtained from private communication with Dmitry Semenov and Thomas Henning. The major dust constituents are “iron-poor” silicates, troilite, organics, and water. Their relative mass fractions are taken from Pollack et al. (1994). These opacities (in  $\text{cm}^2$  per gram of dust) are shown in Figure 2 for the five different grain size bins taken to represent an MRN distribution (see § 4.2 above). The major changes in the dust opacities are: for temperatures  $T < 120$  K, all dust material are present; at  $T \simeq 120$  K, water ice evaporates; at  $T = 275$  K, volatile organics evaporate; at  $T = 450$  K, refractory organics evaporate; at  $T = 680$  K, troilite (FeS) evaporates.

## 7. MODIFIED ZEUS-MP CODE

In order to solve for the evolution of the many complex, nonlinear systems of equations presented in this paper, numerical techniques are necessary. Rather than extend the sophisticated fully implicit, nonorthogonal adaptive mesh, two-fluid MHD code of Fielder & Mouschovias (1992) to include radiative transfer, we have opted instead to modify the publicly-available Zeus-MP RMHD code (Hayes et al. 2006). We have altered the algorithms governing the evolution of the magnetic field in order to account for ambipolar diffusion and Ohmic dissipation. In addition, we have added routines to evolve the total grain density and to compute the species abundances from the equilibrium chemical model detailed in § 4.3, and have made changes to Zeus-MP’s adaptive mesh module in order to track the collapsing core. New modules were also written to improve both the efficiency of Zeus-MP’s implicit radiative transfer solver and the manner in which the gravitational potential is calculated. A brief description of these modifications follows.

The evolution of the magnetic field is governed by equation (35). This equation does not assume flux-freezing in any species and accounts for both ambipolar diffusion and Ohmic dissipation. The first term on the right-hand side,  $\nabla \times (\mathbf{v}_n \times \mathbf{B})$ , represents the advection of the magnetic field by the neutrals. As long as the nonideal MHD Courant condition

$$\Delta t \leq \Delta t_{\text{diff}} \equiv \frac{4\pi}{c^2\eta_{\perp}} \frac{(\Delta x)^2}{2} \quad (67)$$

is satisfied, then the method of characteristics used to update the magnetic field due to this term remains valid (Mac Low et al. 1995) and we may use it without modification. Physically, this is because, for a sufficiently short timestep, ambipolar diffusion

does not have time to alter the characteristics of Alfvén waves. The second term on the right-hand side,  $\nabla \times [(c^2 \eta_{\perp} / 4\pi) \nabla \times \mathbf{B}]$ , represents the diffusion of the magnetic field lines and is applied using the method of constrained transport. This is done in the source step part of the code. We employ a similar approach to the grain continuity equation (58). The right-hand side is treated as a source term in the source step part of the code. Then, the grain mass density is advected during the transport step using the multi-species advection module already present in Zeus-MP. Joule heating (eq. [60]) is also applied to the internal energy during the source step.

We use an adaptive grid to track the evolution of the contracting core. The grid, which must resolve the core, has its innermost zone constrained so as to always have a width in the range  $\lambda_{T,\text{cr}}/5 - \lambda_{T,\text{cr}}/10$ , where  $\lambda_{T,\text{cr}} \equiv 1.4C\tau_{\text{ff}}$  is the critical thermal lengthscale (Mouschovias 1991),  $C \equiv (k_{\text{B}}T/m_{\text{n}})^{1/2}$  is the isothermal sound speed of the gas, and  $\tau_{\text{ff}} \equiv (3\pi/32G\rho_{\text{n},\text{c}})^{1/2}$  is the spherical free-fall time. (The quantity  $\rho_{\text{n},\text{c}}$  is the neutral mass density at the cloud center). The critical thermal lengthscale is the smallest scale on which there can be spatial structure in the density without thermal-pressure forces smoothing it out. The number of cells is fixed, and their positions are spaced logarithmically, so that the spacing between the  $i$ th and  $i$ th + 1 cells is a number greater than the spacing between the  $i$ th - 1 and  $i$ th cells.

As discussed in § 3.8.1 of Hayes et al. (2006), Zeus-MP uses the diagonal preconditioned conjugate gradient method to solve the sparse matrix equation that results from spatially discretizing equations (1m) and (1n). Diagonal preconditioning is an attractive technique due to its simple calculation, the fact that it poses no barrier to parallel implementation, and its fairly common occurrence in linear systems. However, it is only efficient for matrices in which the main diagonal elements are much greater in magnitude than the off-diagonal elements (a condition referred to as “diagonal dominance”). Unfortunately, this is generally not the case for the problem studied here. We have therefore replaced the diagonal preconditioner with an incomplete Cholesky decomposition preconditioner, similar to what was provided in the public-release version of Zeus-2D. The savings in computational cost has been enormous.

Zeus-MP computes the gravitational potential through a two-step process: first, the gravitational potential  $\psi$  is found on the computational boundaries; then  $\psi$  is found in the interior by iteratively solving the Poisson equation for  $\psi$  using a sparse matrix solver that relies on the preconditioned conjugate gradient method. For each boundary of the domain, there are two possible boundary types: (1) Neumann, in which the slope of the gravitational potential is set to zero; and, (2) Dirichlet, in which the value of  $\psi$  in the ghost zones is specified. (There is actually a third possible boundary type — periodic boundary conditions — however, this boundary condition is not used here.) Neumann boundary conditions are used at symmetry boundaries (axis  $r = 0$  and equatorial plane  $z = 0$ ), while Dirichlet conditions are applied at the outer boundaries, far from most of the mass distribution. In the public-release version of Zeus-MP, Dirichlet boundary conditions are implemented by computing  $\psi$  on the domain boundaries using a multipole expansion formula, which we give here in spherical coordinates ( $\varkappa, \theta, \phi$ ) for an axisymmetric mass distribution:

$$\psi(\varkappa, \theta) = -G \sum_{\ell=0,2} \left[ \int \rho(\varkappa', \theta') P_{\ell}(\cos \theta') \varkappa'^{\ell} d^3 \varkappa' \right] \frac{P_{\ell}(\cos \theta)}{\varkappa^{\ell+1}}, \quad (68)$$

where  $P_{\ell}$  is the Legendre polynomial of degree  $\ell$ . Note that Zeus-MP uses only the monopole and quadrupole moments, in contrast to the earlier Zeus-2D code (Stone & Norman 1992), which used arbitrarily high  $\ell$  moments until a desired convergence was achieved. The term in brackets is denoted by  $q_{\ell}$ , and is known as the multipole moment of order  $\ell$  of the density distribution. In most situations, a dozen or so multipole moments are sufficient for convergence. They can be calculated once and then used to find the potential at many boundary points. However, we have found this subroutine inadequate for our purposes, as it fails to converge in situations when the distance  $\varkappa$  to the point at which one wishes to calculate the potential is greater than the distance to any mass element. In the axisymmetric geometry used in this work, this situation is inevitable: mass elements near  $(r, z) = (0, Z)$  or  $(r, z) = (R, 0)$  are closer to the origin than are mass elements near  $(r, z) = (R, Z)$ . We therefore have followed Desch & Mouschovias (2001) in using the more general multipole expansion (Jackson 1999):

$$\psi(\varkappa, \theta) = -G \sum_{\ell=0}^{\infty} \left[ \int \rho(\varkappa', \theta') P_{\ell}(\cos \theta') \frac{\varkappa_{<}^{\ell}}{\varkappa_{>}^{\ell+1}} d^3 \varkappa' \right] P_{\ell}(\cos \theta), \quad (69)$$

where  $\varkappa_{>}$  ( $\varkappa_{<}$ ) is the greater (lesser) of  $\varkappa'$  and  $\varkappa$ , and  $\ell$  may take arbitrarily large integral values until a desired convergence is achieved. An unfortunate consequence of this more general expansion is that it is *not* possible to perform one integration over all space and use the result of that integration (the multipole moment  $q_{\ell}$ ) to find the potential at all boundary points. Instead, a new integration over space must be performed for each boundary point, since the location of that boundary point will determine how the integral in equation (69) is separated into two integrals: one integral will have  $\varkappa'$  in the numerator of the integrand, and in the other integral  $\varkappa'$  will be in the denominator. This situation is further complicated by the use of parallelization, since comparisons of  $\varkappa$  and  $\varkappa'$  and subsequent integrations must take place across multiple processors.

## 8. SUMMARY

We have formulated the problem of the formation and evolution of fragments (or cores) in magnetically-supported, self-gravitating molecular clouds in two spatial dimensions. The evolution is governed by the six-fluid RMHD equations. The magnetic flux is not assumed to be frozen in any of the charged species. Its evolution is determined by a newly-derived generalized Ohm’s law, which accounts for the contributions of both elastic and inelastic collisions to ambipolar diffusion and Ohmic dissipation. The species abundances (electrons, atomic and molecular ions, positively-charged grains, negatively-charged grains, and neutral grains) are calculated using an extensive equilibrium chemical network. Both MRN and uniform grain size distributions are considered. The thermal evolution of the protostellar core and its effect on the dynamics are followed by employing the

grey FLD approximation. Realistic temperature-dependent grain opacities are used that account for a variety of grain compositions. We have augmented the publicly-available Zeus-MP code to take into consideration all these effects and have modified several of its algorithms to increase its accuracy and efficiency.

We summarize here for convenience the simplified evolutionary equations discussed above and used in our modified version of the Zeus-MP code:

$$\frac{\partial \rho_n}{\partial t} + \nabla \cdot (\rho_n \mathbf{v}_n) = 0, \quad (70a)$$

$$\frac{\partial \rho_g}{\partial t} + \nabla \cdot (\rho_g \mathbf{v}_n) = -\nabla \cdot (\eta_{\text{cont,H}} \mathbf{j} \times \mathbf{b}), \quad (70b)$$

$$\frac{\partial (\rho_n \mathbf{v}_n)}{\partial t} + \nabla \cdot (\rho_n \mathbf{v}_n \mathbf{v}_n) = -\nabla P_n - \rho \nabla \psi + \frac{1}{4\pi} (\nabla \times \mathbf{B}) \times \mathbf{B} - \lambda_{\text{FLD}} \nabla \mathcal{E}, \quad (70c)$$

$$\frac{\partial \mathbf{B}}{\partial t} = \nabla \times \left( \mathbf{v}_n \times \mathbf{B} - \frac{c^2 \eta_{\perp}}{4\pi} \nabla \times \mathbf{B} \right), \quad (70d)$$

$$\nabla^2 \psi = 4\pi G \rho_n, \quad (70e)$$

$$\frac{\partial u_n}{\partial t} + \nabla \cdot (u_n \mathbf{v}_n) = -P_n \nabla \cdot \mathbf{v}_n - 4\pi \kappa_P \mathcal{B} + c \kappa_P \mathcal{E}, \quad (70f)$$

$$\frac{\partial \mathcal{E}}{\partial t} + \nabla \cdot (\mathcal{E} \mathbf{v}_n) = \nabla \cdot \left( \frac{c \lambda_{\text{FLD}}}{\chi_R} \nabla \mathcal{E} \right) - \nabla \mathbf{v}_n : \mathbf{P} + 4\pi \kappa_P \mathcal{B} - c \kappa_P \mathcal{E}. \quad (70g)$$

These equations are considered together with the relations  $P_n = (\gamma - 1)u_n$  and  $\mathbf{P} = \mathbf{f}\mathcal{E}$ . Results will be presented in a forthcoming paper (Kunz & Mouschovias 2009, in preparation).

We thank Konstantinos Tassis, Vasiliki Pavlidou, Steve Desch, Leslie Looney, and Duncan Christie for valuable discussions; John Hayes for his assistance with the Zeus-MP code; and, Dmitry Semenov and Thomas Henning for generously providing the dust opacities. TM acknowledges partial support from the National Science Foundation under grant NSF AST-07-09206.

## APPENDIX

### A. RATE COEFFICIENTS

For radiative recombination of atomic ions and electrons,  $\alpha_{\text{rr}} = 2.8 \times 10^{-12} (300 \text{ K}/T)^{0.86} \text{ cm}^3 \text{ s}^{-1}$ ; for the dissociative recombination of electrons and  $\text{HCO}^+$  ions,  $\alpha_{\text{dr}} = 2.0 \times 10^{-7} (300 \text{ K}/T)^{0.75} \text{ cm}^3 \text{ s}^{-1}$  (Umebayashi & Nakano 1990). The rate coefficient adopted for charge exchange reactions between atomic and molecular ions is  $\beta = 2.5 \times 10^{-9} \text{ cm}^3 \text{ s}^{-1}$  (Watson 1976).

The rate coefficients involving gas-phase species and grains are taken from Spitzer (1941, 1948), with refinements made by Draine & Sutin (1987) to account for the polarization of grains:

$$\alpha_{\text{ego}} = \pi a^2 \left( \frac{8k_B T}{\pi m_e} \right)^{1/2} \left[ 1 + \left( \frac{\pi e^2}{2ak_B T} \right)^{1/2} \right] \mathcal{P}_e, \quad (A1)$$

$$\alpha_{\text{igo}} = \pi a^2 \left( \frac{8k_B T}{\pi m_i} \right)^{1/2} \left[ 1 + \left( \frac{\pi e^2}{2ak_B T} \right)^{1/2} \right] \mathcal{P}_i, \quad (A2)$$

$$\alpha_{\text{eg}+} = \pi a^2 \left( \frac{8k_B T}{\pi m_e} \right)^{1/2} \left[ 1 + \left( \frac{e^2}{ak_B T} \right) \right] \left[ 1 + \left( \frac{2}{2 + (ak_B T/e^2)} \right)^{1/2} \right] \mathcal{P}_e, \quad (A3)$$

$$\alpha_{\text{ig}-} = \pi a^2 \left( \frac{8k_B T}{\pi m_i} \right)^{1/2} \left[ 1 + \left( \frac{e^2}{ak_B T} \right) \right] \left[ 1 + \left( \frac{2}{2 + (ak_B T/e^2)} \right)^{1/2} \right] \mathcal{P}_i. \quad (A4)$$

The sticking probabilities of electrons or ions onto grains, denoted  $\mathcal{P}_e$  and  $\mathcal{P}_i$ , are assigned the values 0.6 and 1.0, respectively (Umebayashi 1983). Other quantities in these equations have their usual meanings.

The rate coefficients for charge transfer between charged grains are given by

$$\alpha_{\text{g}_+^{\alpha} \text{g}_-^{\alpha'}} = \pi a_{\text{sum}}^2 \left( \frac{8k_B T}{\pi m_{\text{red}}} \right)^{1/2} \left[ 1 + \left( \frac{e^2}{a_{\text{sum}} k_B T} \right) \right] \left[ 1 + \left( \frac{2}{2 + (a_{\text{sum}} k_B T/e^2)} \right)^{1/2} \right], \quad (A5)$$

$$\alpha_{\text{g}_{\pm}^{\alpha} \text{g}_0^{\alpha'}} = \pi a_{\text{sum}}^2 \left( \frac{8k_B T}{\pi m_{\text{red}}} \right)^{1/2} \left[ 1 + \left( \frac{\pi e^2}{2a_{\text{sum}} k_B T} \right)^{1/2} \right] \mathcal{P}_{\alpha\alpha'}, \quad (A6)$$

where the reduced mass of the two grains (labeled  $\alpha$  and  $\alpha'$ ) is defined by  $m_{\text{red}} = m_{\alpha} m_{\alpha'} / (m_{\alpha} + m_{\alpha'})$ , and  $a_{\text{sum}} = a_{\alpha} + a_{\alpha'}$  is the sum of the radii of two grains  $\alpha$  and  $\alpha'$ . The probability of two oppositely charged grains neutralizing each other upon contact is assumed to be unity. The probability of charge being transferred to a neutral grain  $\text{g}_0^{\alpha}$  from a charged grain  $\text{g}_{\pm}^{\alpha'}$  is assumed to be proportional to the surface areas of the grains, so that  $\mathcal{P}_{\alpha\alpha'} = a_{\alpha\alpha'}^2 / (a_{\alpha}^2 + a_{\alpha'}^2)$ . In other words, of all the collisions between a neutral grain,  $\alpha$ , and a charged grain,  $\alpha'$ , only a fraction  $\mathcal{P}_{\alpha}$  lead to charge exchange. The complementary probability  $\mathcal{P}_{\alpha'}$  leaves the charges unchanged.

## B. GENERALIZED OHM'S LAW

## B.1. Derivation

We consider equations (42) and (43), repeated here for convenience, which are to be solved for the species drift velocities  $\mathbf{w}_s$  relative to the neutrals:

$$0 = \frac{\omega_s \tau_{sn}}{1 + \varrho_s} \left( \frac{c}{B} \mathbf{E}_n + \mathbf{w}_s \times \mathbf{b} \right) - \mathbf{w}_s + \frac{\varrho_s}{1 + \varrho_s} \mathbf{w}_{g_0}, \quad (\text{B1})$$

$$0 = \mathbf{w}_{g_0} - \sum_k \frac{\tau_0}{\tau_{k,\text{inel}}} \mathbf{w}_k. \quad (\text{B2})$$

We define, for brevity and clarity of presentation, the following quantities

$$\Psi_{1,s} = \frac{\frac{\tau_0}{\tau_{s,\text{inel}}} \frac{\omega_s \tau_{sn}}{1 + \varrho_s}}{1 - \sum_k \frac{\tau_0}{\tau_{k,\text{inel}}} \frac{\varrho_k}{1 + \varrho_k}}, \quad \Psi_1 = \sum_k \Psi_{1,k}; \quad (\text{B3a})$$

$$\Psi_{2,s} = \frac{\frac{\tau_0}{\tau_{s,\text{inel}}} \frac{\omega_s^2 \tau_{sn}^2}{(1 + \varrho_s)^2}}{1 - \sum_k \frac{\tau_0}{\tau_{k,\text{inel}}} \frac{\varrho_k}{1 + \varrho_k}}, \quad \Psi_2 = \sum_k \Psi_{2,k}; \quad (\text{B3b})$$

$$\Psi_{3,s} = \frac{\frac{\tau_0}{\tau_{s,\text{inel}}} \frac{\omega_s \tau_{sn}}{1 + \varrho_s} \frac{\varrho_s}{1 + \varrho_s}}{1 - \sum_k \frac{\tau_0}{\tau_{k,\text{inel}}} \frac{\varrho_k}{1 + \varrho_k}}, \quad \Psi_3 = \sum_k \Psi_{3,k}. \quad (\text{B3c})$$

We recall that the index  $k$  runs over all the charged species independently of the index  $s$ , which denotes the charged species in question. Note that the denominator in the above expressions may be written with the help of equation (44b) as

$$\frac{\tau_0}{\tau_{g_0n}} + \sum_k \frac{\tau_0}{\tau_{k,\text{inel}}} \frac{1}{1 + \varrho_k}, \quad (\text{B4})$$

which shows its positive definite nature.

We first multiply equation (B1) by  $\tau_0/\tau_{s,\text{inel}}$ , sum over  $s$ , and use equation (B2) to find that

$$\mathbf{w}_{g_0} = \Psi_1 \frac{c}{B} \mathbf{E}_n + \sum_k \Psi_{1,k} \mathbf{w}_k \times \mathbf{b}, \quad (\text{B5})$$

where we have switched the summation index to  $k$  to avoid confusion with the species in question,  $s$ . Next we take the cross product of equations (B1) and (B5) and the unit vector  $\mathbf{b}$ :

$$\mathbf{w}_s \times \mathbf{b} = \frac{\omega_s \tau_{sn}}{1 + \varrho_s} \left( \frac{c}{B} \mathbf{E}_n \times \mathbf{b} - \mathbf{w}_{s,\perp} \right) + \frac{\varrho_s}{1 + \varrho_s} \mathbf{w}_{g_0} \times \mathbf{b}, \quad (\text{B6})$$

$$\mathbf{w}_{g_0} \times \mathbf{b} = \Psi_1 \frac{c}{B} \mathbf{E}_n \times \mathbf{b} - \sum_k \Psi_{1,k} \mathbf{w}_{k,\perp}. \quad (\text{B7})$$

Equation (B7) is now substituted in equation (B6) to obtain

$$\mathbf{w}_s \times \mathbf{b} = \left( \frac{\omega_s \tau_{sn}}{1 + \varrho_s} + \frac{\varrho_s}{1 + \varrho_s} \Psi_1 \right) \frac{c}{B} \mathbf{E}_n \times \mathbf{b} - \left( \frac{\omega_s \tau_{sn}}{1 + \varrho_s} \mathbf{w}_{s,\perp} + \frac{\varrho_s}{1 + \varrho_s} \sum_k \Psi_{1,k} \mathbf{w}_{k,\perp} \right). \quad (\text{B8})$$

Inserting this expression in equation (B5), we find that

$$\mathbf{w}_{g_0} = \Psi_1 \frac{c}{B} \mathbf{E}_n + (\Psi_2 + \Psi_3 \Psi_1) \frac{c}{B} \mathbf{E}_n \times \mathbf{b} - \sum_k (\Psi_{2,k} + \Psi_3 \Psi_{1,k}) \mathbf{w}_{k,\perp}, \quad (\text{B9})$$

which is now ready to be inserted, along with equation (B8), in equation (B1):

$$\begin{aligned} \mathbf{w}_s + \sum_k \left[ \frac{\omega_s \tau_{sn}}{1 + \varrho_s} \left( \frac{\omega_k \tau_{kn}}{1 + \varrho_k} \delta_{sk} + \frac{\varrho_s}{1 + \varrho_s} \Psi_{1,k} \right) + \frac{\varrho_s}{1 + \varrho_s} (\Psi_{2,k} + \Psi_3 \Psi_{1,k}) \right] \mathbf{w}_{k,\perp} \\ = \left( \frac{\omega_s \tau_{sn}}{1 + \varrho_s} + \frac{\varrho_s}{1 + \varrho_s} \Psi_1 \right) \frac{c}{B} \mathbf{E}_n + \left[ \frac{\omega_s \tau_{sn}}{1 + \varrho_s} \left( \frac{\omega_s \tau_{sn}}{1 + \varrho_s} + \frac{\varrho_s}{1 + \varrho_s} \Psi_1 \right) + \frac{\varrho_s}{1 + \varrho_s} (\Psi_2 + \Psi_3 \Psi_1) \right] \frac{c}{B} \mathbf{E}_n \times \mathbf{b}. \end{aligned} \quad (\text{B10})$$



The symbol  $\delta_{sk}$  is the Kronecker delta. This is our first main result: it gives the velocity of each charged species in terms of the electric field in the frame of the neutrals. Another way of interpreting this equation is obtained by defining the velocity of the magnetic field lines with respect to the lab frame:

$$\mathbf{v}_f \equiv \frac{c}{B} \mathbf{E} \times \mathbf{b}. \quad (\text{B11})$$

Then equation (B10) provides the velocities of all the charged species in terms of the neutral velocity and the field-line velocity. We made use of this concept earlier in Section 5.3.

Equation (B10) can be separated into components parallel and perpendicular to the magnetic field. The parallel component of the current density is easily obtained:

$$\mathbf{j}_{||} = \sum_s n_s q_s \mathbf{w}_{s,||} \quad (\text{B12a})$$

$$= \sum_s n_s q_s \left( \frac{\omega_s \tau_{sn}}{1 + \varrho_s} + \frac{\varrho_s}{1 + \varrho_s} \Psi_1 \right) \frac{c}{B} \mathbf{E}_{n,||} \quad (\text{B12b})$$

$$= \sum_s \sigma_s (1 - \varsigma_s) \mathbf{E}_{n,||} \quad (\text{B12c})$$

$$\equiv \sigma_{||} \mathbf{E}_{n,||}, \quad (\text{B12d})$$

where we have introduced the conductivity of species  $s$ ,  $\sigma_s = n_s q_s^2 \tau_{sn} / m_s$ , and  $\varsigma_s$ , given in Appendix D, is the factor by which the conductivity of species  $s$  is altered because of inelastic collisions. In the last step above, we have introduced the parallel conductivity,  $\sigma_{||}$ , which is defined *in situ*. Note that  $\varsigma_s \geq 0$  for all  $s$ . In other words, by interfering with the rate at which the charge carriers flow along the magnetic field, inelastic collisions are responsible for decreasing (increasing) the parallel conductivity (resistivity) of the gas.

Finding the perpendicular components of the current density is not as straightforward and amounts to solving a matrix equation. We first define the  $4 \times 1$  column vectors  $\mathbf{C}^\perp$  and  $\mathbf{C}^\text{H}$ , whose entries are given by

$$(\mathbf{C}^\perp)_s = \omega_s \tau_{sn} (1 - \varsigma_s) \quad \text{and} \quad (\mathbf{C}^\text{H})_s = -\omega_s^2 \tau_{sn}^2 (1 - \varpi_s). \quad (\text{B13a,b})$$

We also define the  $4 \times 4$  matrix of coefficients  $\mathbf{A}$  whose entries are given by

$$(\mathbf{A})_{sk} = [1 + \omega_s^2 \tau_{sn}^2 (1 - \varphi_s)] \delta_{sk} + \omega_k^2 \tau_{kn}^2 \vartheta_{sk} (1 - \delta_{sk}). \quad (\text{B14})$$

The expressions for  $\varsigma_s$ ,  $\varpi_s$ ,  $\varphi_s$ , and  $\vartheta_{sk}$  are given below in Appendix D. Then the perpendicular component of equation (B10) takes on the form

$$\mathbf{C}^\perp \frac{c}{B} \mathbf{E}_{n,\perp} - \mathbf{C}^\text{H} \frac{c}{B} \mathbf{E}_n \times \mathbf{b} = \mathbf{A} \mathbf{W}_\perp, \quad (\text{B15})$$

where  $\mathbf{W}_\perp$  is the  $4 \times 1$  column vector of unknown velocities of charge species relative to neutrals,  $[\mathbf{w}_e, \mathbf{w}_i, \mathbf{w}_{g_-}, \mathbf{w}_{g_+}]^\text{T}$ .

We use Cramer's method to solve the matrix equation (B15). We define

$$D = \det[\mathbf{A}]. \quad (\text{B16})$$

In addition, we use the notation  $D_s^\perp$  to represent the determinant of  $\mathbf{A}$  with the  $s$ th column of  $\mathbf{A}$  having been replaced by  $\mathbf{C}^\perp$ . Similarly,  $D_s^\text{H}$  is the determinant of  $\mathbf{A}$  with the  $s$ th column having been replaced by  $\mathbf{C}^\text{H}$ . Then, the solution of the system (B15) is

$$\mathbf{w}_{s,\perp} = \frac{D_s^\perp}{D} \frac{c}{B} \mathbf{E}_{n,\perp} - \frac{D_s^\text{H}}{D} \frac{c}{B} \mathbf{E}_n \times \mathbf{b}. \quad (\text{B17})$$

Once the determinants have been computed, the current density perpendicular to the magnetic field may be obtained:

$$\mathbf{j}_\perp = \sum_s n_s q_s \mathbf{w}_{s,\perp} \quad (\text{B18a})$$

$$= \frac{\sum_s n_s q_s D_s^\perp}{D} \frac{c}{B} \mathbf{E}_{n,\perp} - \frac{\sum_s n_s q_s D_s^\text{H}}{D} \frac{c}{B} \mathbf{E}_n \times \mathbf{b} \quad (\text{B18b})$$

$$= \sum_s \frac{\sigma_s (1 - \varsigma_s)}{1 + \omega_s^2 \tau_{sn}^2 (1 - \varphi_s)} \Upsilon(\varsigma) \mathbf{E}_{n,\perp} + \sum_s \frac{\sigma_s \omega_s \tau_{sn} (1 - \varpi_s)}{1 + \omega_s^2 \tau_{sn}^2 (1 - \varphi_s)} \Upsilon(\varpi) \mathbf{E}_n \times \mathbf{b} \quad (\text{B18c})$$

$$\equiv \sigma_\perp \mathbf{E}_{n,\perp} - \sigma_\text{H} \mathbf{E}_n \times \mathbf{b}. \quad (\text{B18d})$$

In the last step, we have defined the perpendicular conductivity  $\sigma_\perp$  and the Hall conductivity  $\sigma_\text{H}$ , which include the effects of inelastic collisions.

### B.2. Modification due to a Grain Size Distribution

When considering a grain size distribution, rather than single-size grains, two changes must be made to the above derivation. First, the inelastic collision timescales given by equations (39) and (40) must be modified as follows:

$$\tau_{g_+,inel} \rightarrow \tau_{g_+^{\alpha},inel} = \left[ \frac{1}{\tau_{g_0^{\alpha}i,incl}} + \frac{\rho_{g_+^{\alpha}}}{\rho_{g_0^{\alpha}}} \frac{1}{\tau_{g_+^{\alpha}e,incl}} + \sum_{\alpha'} \left( \frac{1}{\tau_{g_0^{\alpha}g_+^{\alpha'},inel}} + \frac{\rho_{g_+^{\alpha}}}{\rho_{g_0^{\alpha}}} \frac{1}{\tau_{g_+^{\alpha}g_0^{\alpha'},inel}} + \frac{\rho_{g_+^{\alpha}}}{\rho_{g_0^{\alpha}}} \frac{1}{\tau_{g_+^{\alpha}g_+^{\alpha'},inel}} \right) \right]^{-1}, \quad (B19a)$$

$$\tau_{g_-,inel} \rightarrow \tau_{g_-^{\alpha},inel} = \left[ \frac{1}{\tau_{g_0^{\alpha}e,incl}} + \frac{\rho_{g_-^{\alpha}}}{\rho_{g_0^{\alpha}}} \frac{1}{\tau_{g_-^{\alpha}i,incl}} + \sum_{\alpha'} \left( \frac{1}{\tau_{g_0^{\alpha}g_-^{\alpha'},inel}} + \frac{\rho_{g_-^{\alpha}}}{\rho_{g_0^{\alpha}}} \frac{1}{\tau_{g_-^{\alpha}g_0^{\alpha'},inel}} + \frac{\rho_{g_-^{\alpha}}}{\rho_{g_0^{\alpha}}} \frac{1}{\tau_{g_-^{\alpha}g_+^{\alpha'},inel}} \right) \right]^{-1}. \quad (B19b)$$

The summations over  $\alpha'$  (the grain size label) indicate that a grain of size  $\alpha$  may give or receive charges not only from other grains of its own size, but also from all other different-size grains. Second, the summation index  $s$  in equations (B12) and (B18) should range over *all* charged species, including all sizes of charged grains.

### C. DERIVATION OF SPECIES VELOCITIES

En route to the derivation of a generalized Ohm's law, the differential velocity of every species can be obtained in terms of the current density:

$$\begin{aligned} n_s q_s \mathbf{w}_s &= \sigma_{||,s} \mathbf{E}_{n,||} + \sigma_{\perp,s} \mathbf{E}_{n,\perp} - \sigma_{H,s} \mathbf{E}_n \times \mathbf{b} \\ &= \sigma_{||,s} \eta_{||} \mathbf{j}_{||} + \sigma_{\perp,s} (\eta_{\perp} \mathbf{j}_{\perp} + \eta_H \mathbf{j} \times \mathbf{b}) - \sigma_{H,s} (\eta_{\perp} \mathbf{j} \times \mathbf{b} - \eta_H \mathbf{j}_{\perp}) \\ &= \sigma_{||,s} \eta_{||} \mathbf{j}_{||} + (\sigma_{\perp,s} \eta_{\perp} + \sigma_{H,s} \eta_H) \mathbf{j}_{\perp} + (\sigma_{\perp,s} \eta_H - \sigma_{H,s} \eta_{\perp}) \mathbf{j} \times \mathbf{b}. \end{aligned} \quad (C1)$$

Using equation (B11), it is straightforward to show that

$$\mathbf{w}_f \equiv \mathbf{v}_f - \mathbf{v}_n = \frac{c\eta_{\perp}}{B} \mathbf{j} \times \mathbf{b} - \frac{c\eta_H}{B} \mathbf{j}_{\perp}. \quad (C2)$$

We may then write the components of the current density in terms of the differential velocity of the field lines as

$$\frac{c}{B} \mathbf{j} \times \mathbf{b} = \sigma_{\perp} \mathbf{w}_{f,\perp} - \sigma_H \mathbf{w}_f \times \mathbf{b} \quad \text{and} \quad -\frac{c}{B} \mathbf{j}_{\perp} = \sigma_H \mathbf{w}_{f,\perp} + \sigma_{\perp} \mathbf{w}_f \times \mathbf{b}. \quad (C3a,b)$$

Defining the indirect coupling coefficient  $\Theta_s$  implicitly by

$$\frac{\Theta_s}{\Theta_s + 1} \equiv \left( \frac{B}{cn_s q_s} \right) [\sigma_{\perp} (\sigma_{\perp,s} \eta_H - \sigma_{H,s} \eta_{\perp}) - \sigma_H (\sigma_{\perp,s} \eta_{\perp} + \sigma_{H,s} \eta_H)], \quad (C4)$$

and introducing

$$\Lambda_s \equiv - \left( \frac{B}{cn_s q_s} \right) [\sigma_{\perp} (\sigma_{\perp,s} \eta_{\perp} + \sigma_{H,s} \eta_H) + \sigma_H (\sigma_{\perp,s} \eta_H - \sigma_{H,s} \eta_{\perp})], \quad (C5)$$

equation (C1) may now be written in component form as

$$\mathbf{w}_{s,\perp} = \frac{\Theta_s}{\Theta_s + 1} \mathbf{w}_{f,\perp} + \Lambda_s \mathbf{w}_f \times \mathbf{b} \quad \text{and} \quad \mathbf{w}_s \times \mathbf{b} = \frac{\Theta_s}{\Theta_s + 1} \mathbf{w}_f \times \mathbf{b} - \Lambda_s \mathbf{w}_{f,\perp}, \quad (C6a,b)$$

or, more explicitly,

$$\mathbf{v}_{s,\perp} = \mathbf{v}_{n,\perp} \frac{1}{\Theta_s + 1} + \mathbf{v}_{f,\perp} \frac{\Theta_s}{\Theta_s + 1} + (\mathbf{v}_f - \mathbf{v}_n) \times \mathbf{b} \Lambda_s, \quad (C7a)$$

$$\mathbf{v}_s \times \mathbf{b} = \mathbf{v}_n \times \mathbf{b} \frac{1}{\Theta_s + 1} + \mathbf{v}_f \times \mathbf{b} \frac{\Theta_s}{\Theta_s + 1} - (\mathbf{v}_{f,\perp} - \mathbf{v}_{n,\perp}) \Lambda_s. \quad (C7b)$$

These equations were discussed in Section 5.3.

### D. DEFINITIONS

In the main text, as well as in the preceding appendices, we had delayed giving explicit definitions of  $\zeta_s$ ,  $\varpi_s$ ,  $\varphi_s$ ,  $\Upsilon_s$ , and  $\vartheta_{sk}$  for all  $(s, k) = e, i, g_-,$  and  $g_+$  due to their complexity and length. Here we give explicit expressions for these quantities for all the charged species. Before we proceed, however, a few simplifications are in order. Since both  $(\tau_{e,incl}/\tau_{en})$  and  $(\tau_{i,incl}/\tau_{in}) \gg 1$  for the density regime of interest in this paper, we may neglect the influence of inelastic collisions on the electron and ion fluids. Using the results of Tassis & Mouschovias (2007b), we also may assume that the velocity difference between a given grain and a neutral particle is less than the sound speed of the gas. These are both excellent assumptions, and lead to a much more compact form of the following definitions than would otherwise be possible.

The variable  $\zeta_s$  first appeared in the definition of the parallel conductivity (B12) and again later in the definition of the perpendicular conductivity (B18). For electrons and ions,  $\zeta_e = \zeta_i = 0$ , because of the negligible influence of inelastic collisions on the electron and ion fluids relative to that of elastic collisions. The expressions for the negative and positive grains are given by

$$\zeta_{g_{\pm}} = \frac{\varrho_{g_{\pm}}}{1 + \varrho_{g_{\pm}}} \left[ \frac{\frac{\tau_0}{\tau_{g_0n}} + \frac{\tau_0}{\tau_{g_{\mp},inel}} \frac{2}{1 + \varrho_{g_{\mp}}}}{\frac{\tau_0}{\tau_{g_0n}} + \frac{\tau_0}{\tau_{g_+,inel}} \frac{1}{1 + \varrho_{g_+}} + \frac{\tau_0}{\tau_{g_-,inel}} \frac{1}{1 + \varrho_{g_-}}} \right], \quad (D1)$$

and are clearly positive. As mentioned in Section 5.2, by interfering with the rate at which the charge carriers flow along the magnetic field, inelastic collisions are responsible for decreasing (increasing) the parallel conductivity (resistivity) of the gas.

The derivation of the perpendicular conductivity involved many more definitions, all of which are given below. For the same reason stated above for which  $\varsigma_e = \varsigma_i = 0$ , the expressions for  $\varpi_s$  and  $\varphi_s$  vanish when  $s = e$  or  $i$ . The quantity  $\Upsilon_s$  is equal to unity for these species. The nontrivial  $\varpi_s$ ,  $\varphi_s$ , and  $\Upsilon_s$  for  $s = g_-, g_+$  are given by

$$\varpi_{g\pm} = \frac{\varsigma_{g\pm}}{1 + \varrho_{g\pm}} + \frac{\varrho_{g\mp}}{1 + \varrho_{g\mp}} \left[ \frac{\frac{\tau_0}{\tau_{g0n}} + \frac{\tau_0}{\tau_{g+,inel}} \frac{\varsigma_{g+}}{1 + \varrho_{g+}} + \frac{\tau_0}{\tau_{g-,inel}} \frac{\varsigma_{g-}}{1 + \varrho_{g-}}}{\frac{\tau_0}{\tau_{g0n}} + \frac{\tau_0}{\tau_{g+,inel}} \frac{1}{1 + \varrho_{g+}} + \frac{\tau_0}{\tau_{g-,inel}} \frac{1}{1 + \varrho_{g-}}} \right]; \quad (D2)$$

$$\varphi_{g\pm} = \frac{\varrho_{g\pm}}{1 + \varrho_{g\pm}} \frac{2 + \varrho_{g\pm}}{1 + \varrho_{g\pm}} \left[ \frac{\frac{\tau_0}{\tau_{g0n}} + \frac{\tau_0}{\tau_{g\mp,incl}} \frac{1}{1 + \varrho_{g\mp}}}{\frac{\tau_0}{\tau_{g0n}} + \frac{\tau_0}{\tau_{g+,inel}} \frac{1}{1 + \varrho_{g+}} + \frac{\tau_0}{\tau_{g-,inel}} \frac{1}{1 + \varrho_{g-}}} \right] + \frac{\tau_0}{\tau_{g\pm,incl}} \frac{\varrho_{g\pm}}{(1 + \varrho_{g\pm})^2} \left[ \frac{\frac{\tau_0}{\tau_{g0n}} \frac{\varrho_{g\pm}}{1 + \varrho_{g\pm}} + \frac{\tau_0}{\tau_{g\mp,incl}} \frac{1}{1 + \varrho_{g\mp}} \left( \frac{\varrho_{g+}}{1 + \varrho_{g+}} + \frac{\varrho_{g-}}{1 + \varrho_{g-}} \right)}{\left( \frac{\tau_0}{\tau_{g0n}} + \frac{\tau_0}{\tau_{g+,inel}} \frac{1}{1 + \varrho_{g+}} + \frac{\tau_0}{\tau_{g-,inel}} \frac{1}{1 + \varrho_{g-}} \right)^2} \right]; \quad (D3)$$

$$\Upsilon_{g\pm}(\varsigma) = \frac{1 + \frac{\omega_{g\mp}^2 \tau_{g\mp n}^2 \vartheta_{g\pm g\mp}}{1 + \omega_{g\mp}^2 \tau_{g\mp n}^2 (1 - \varphi_{g\mp})} \frac{1 - \varsigma_{g\mp}}{1 - \varsigma_{g\pm}}}{1 - \frac{\omega_{g+}^2 \tau_{g+n}^2 \vartheta_{g-g+}}{1 + \omega_{g+}^2 \tau_{g+n}^2 (1 - \varphi_{g+})} \frac{\omega_{g-}^2 \tau_{g-n}^2 \vartheta_{g+g-}}{1 + \omega_{g-}^2 \tau_{g-n}^2 (1 - \varphi_{g-})}}; \quad (D4)$$

$$\Upsilon_{g\pm}(\varpi) = \frac{1 + \frac{\omega_{g\mp}^2 \tau_{g\mp n}^2 \vartheta_{g\pm g\mp}}{1 + \omega_{g\mp}^2 \tau_{g\mp n}^2 (1 - \varphi_{g\mp})} \frac{1 - \varpi_{g\mp}}{1 - \varpi_{g\pm}}}{1 - \frac{\omega_{g+}^2 \tau_{g+n}^2 \vartheta_{g-g+}}{1 + \omega_{g+}^2 \tau_{g+n}^2 (1 - \varphi_{g+})} \frac{\omega_{g-}^2 \tau_{g-n}^2 \vartheta_{g+g-}}{1 + \omega_{g-}^2 \tau_{g-n}^2 (1 - \varphi_{g-})}}. \quad (D5)$$

In equation (B14), we had introduced  $\vartheta_{sk}$  as a measure of the inelastic collisional coupling between different pairs of charged species,  $s \neq k$ . This variable was also used in the definition of  $\Upsilon_s$  above. Since the effect of inelastic collisions on the electron and ion fluids is negligible,  $\vartheta_{sk}$  vanishes for  $(s, k) = e$  or  $i$ . The only remaining nonzero values of  $\vartheta_{sk}$  involve the charged grain species, and are given by

$$\vartheta_{g\pm g\mp} = \frac{\varrho_{g\pm}}{1 + \varrho_{g\pm}} \frac{\tau_0}{\tau_{g\mp,incl}} \frac{1}{1 + \varrho_{g\mp}} \left[ \frac{\frac{1}{1 + \varrho_{g\mp}} \left( 1 - \frac{\tau_0}{\tau_{g\pm,incl}} \frac{\varrho_{g\pm}}{1 + \varrho_{g\pm}} \right) - \frac{1}{1 + \varrho_{g\pm}} \left( 1 - \frac{\tau_0}{\tau_{g\mp,incl}} \frac{\varrho_{g\mp}}{1 + \varrho_{g\mp}} \right)}{\left( \frac{\tau_0}{\tau_{g0n}} + \frac{\tau_0}{\tau_{g+,inel}} \frac{1}{1 + \varrho_{g+}} + \frac{\tau_0}{\tau_{g-,inel}} \frac{1}{1 + \varrho_{g-}} \right)^2} \right]. \quad (D6)$$

## REFERENCES

- Adams, F., & Shu, F. H. 1985, *ApJ*, 296, 655  
Adams, F., & Shu, F. H. 1986, *ApJ*, 308, 836  
Alves, F. O., Franco, G. A. P., & Girart, J. M. 2008, *A&A*, 486, L13  
Arons, J., & Max, C. E. 1975, *ApJ*, 196, L77  
Babcock, H. W., & Cowling, T. G. 1953, *MNRAS*, 113, 357  
Bacmann, A., André, P., Puget, J. L., Abergel, A., Bontemps, S., & Ward-Thompson, D. 2000, *A&A*, 361, 555  
Baker, P. L. 1979, *A&A*, 75, 54  
Basu, S., & Mouschovias, T. Ch. 1994, *ApJ*, 432, 720  
Basu, S., & Mouschovias, T. Ch. 1995a, *ApJ*, 452, 386  
Basu, S., & Mouschovias, T. Ch. 1995b, *ApJ*, 453, 271  
Bate, M. R. 1998, *ApJ*, 508, L95  
Baudry, A., Perault, M., de La Noe, J., Despois, D., Cernicharo, J. 1981, *A&A*, 104, 101  
Black, D. C., & Bodenheimer, P. 1975, *ApJ*, 199, 619  
Black, D. C., & Bodenheimer, P. 1976, *ApJ*, 206, 138  
Bodenheimer, P. 1968, *ApJ*, 153, 483  
Bodenheimer, P., Yorke, H. W., & Laughlin, G. 1993, *ApJ*, 411, 274  
Bodenheimer, P., Yorke, H. W., & Laughlin, G. 1995, *ApJ*, 443, 199  
Bodenheimer, P., Yorke, H. W., Różyska, M., & Tohline, J. E. 1990, *ApJ*, 355, 651  
Boss, A. P. 1981, *ApJ*, 250, 636  
Boss, A. P. 1984, *ApJ*, 277, 768  
Boss, A. P. 1986, *ApJS*, 62, 519  
Boss, A. P. 1988, *ApJ*, 331, 370  
Boss, A. P., & Myhill, E. A. 1995, 451, 218  
Boss, A. P., & Yorke, H. W. 1990, *ApJ*, 353, 236  
Chandrasekhar, S., & Fermi, E. 1953, *ApJ*, 118, 116  
Ciolek, G. E., & Königl, A. 1998, *ApJ*, 504, 257  
Ciolek, G. E., & Mouschovias, T. Ch. 1993, *ApJ*, 418, 774  
Ciolek, G. E., & Mouschovias, T. Ch. 1994, *ApJ*, 425, 142  
Ciolek, G. E., & Mouschovias, T. Ch. 1995, *ApJ*, 454, 194  
Ciolek, G. E., & Mouschovias, T. Ch. 1996, *ApJ*, 468, 749  
Ciolek, G. E., & Mouschovias, T. Ch. 1998, *ApJ*, 504, 280  
Clayton, D. D., & Leising, M. D. 1987, *Phys. Rep.*, 144, 1  
Consolmagno, G. J., & Jopipii, J. R. 1978, *The Moon and the Planets*, 19, 253  
Cortes, P. C., & Crutcher, R. M. 2006, *ApJ*, 639, 965  
Cortes, P. C., Crutcher, R. M., & Watson, W. D. 2005, *ApJ*, 628, 780  
Crutcher, R. M. 1999, *ApJ*, 520, 706  
Crutcher, R. M., & Kazès, I. 1983, *A&A*, 125, L23

- Crutcher, R. M., Mouschovias, T. Ch., Troland, T. H., & Ciolek, G. E. 1994, *ApJ*, 427, 839
- Crutcher, R. M., Nutter, D. J., Ward-Thompson, D., & Kirk, J. M. 2004, *ApJ*, 600, 279
- Crutcher, R. M., Roberts, D. A., Mehringer, D. M., & Troland, T. H. 1996, *ApJ*, 462, L79
- Crutcher, R. M., Roberts, D. A., Troland, T. H., & Goss, W. M. 1999a, *ApJ*, 515, 275
- Crutcher, R. M., Troland, T. H., Goodman, A. A., Heiles, C., Kazès, I., & Myers, P. C. 1993, *ApJ*, 407, 175
- Crutcher, R. M., Troland, T. H., & Kazès, I. 1987, *A&A*, 181, 119
- Crutcher, R. M., Troland, T. H., Lazareff, B., Paubert, G., & Kazès, I. 1999b, *ApJ*, 514, L121
- Desch, S. J., & Mouschovias, T. Ch. 2001, *ApJ*, 550, 314
- Draine, B. T., & Sutin, B. 1987, *ApJ*, 320, 803
- Elmegreen, B. G. 1979, *ApJ*, 232, 729
- Elmegreen, B. G. 1986, in *Light on Dark Matter*, ed. F. P. Israel (Dordrecht: Reidel), 265
- Elmegreen, B. G., & Scalo, J. 2004, *ARA&A*, 42, 211
- Eng, C. 2002, Ph.D. Thesis, University of Illinois at Urbana-Champaign
- Fiedler, R. A., & Mouschovias, T. Ch. 1992, *ApJ*, 391, 199
- Fiedler, R. A., & Mouschovias, T. Ch. 1993, *ApJ*, 415, 680
- Gaustad, J. E. 1963, *ApJ*, 138, 1050
- Girart, J. M., Crutcher, R. M., & Rao, R. 1999, *ApJ*, 525, L109
- Girart, J. M., Rao, R., & Marrone, D. P. 2006, *Science*, 313, 812
- Glassgold, A. E. 1995, *ApJ*, 438, L111
- Glassgold, A. E., & Langer, W. D. 1974, *ApJ*, 193, 73
- Goldreich, P., & Reisenegger, A. 1992, *ApJ*, 395, 250
- Goldsmith, P. F., & Arquilla, R. 1985, in *Protostars and Planets II*, ed. D. C. Black & M. S. Mathews (Tucson: University of Arizona Press), 137
- Goodman, A. A., Crutcher, R. M., Heiles, C., Myers, P. C., & Troland, T. H. 1989, *ApJ*, 338, L61
- Hayashi, C. 1966, *ARA&A*, 4, 171
- Hayes, J. C., Norman, M. L., Fiedler, R. A., Bordner, J. O., Li, P. S., Clark, S. E., ud-Doula, A., & Mac Low, M.-M. 2006, *ApJS*, 165, 188
- Heiles, C. 1987, in *Physical Processes in Interstellar Clouds*, ed. G. E. Morfill & M. Scholer (Dordrecht: Reidel), 429
- Heiles, C., & Crutcher, R. 2005, in *Cosmic Magnetic Fields*, ed. R. Wielebinski & R. Beck (Berlin: Springer), 137
- Heyer, M. H., Vrba, F. J., Snell, R. L., Schloerb, F. P., Strom, S. E., Goldsmith, P. F., & Strom, K. M. 1987, *ApJ*, 321, 855
- Hildebrand, R. H., Dotson, J. L., Dowell, C. D., Schleuning, D. A., & Vaillancourt, J. E. 1999, *ApJ*, 516, 834
- Hollenbach, D. J., Werner, M. W., & Salpeter, E. E. 1971, *ApJ*, 163, 165
- Jackson, J. D. 1999, *Classical Electrodynamics* (3rd ed.; New York: John Wiley & Sons)
- Kazès, I., & Crutcher, R. M. 1986, *A&A*, 164, 328
- Kittel, C. 1958, *Elementary Statistical Physics* (New York: John Wiley & Son)
- Lai, S.-P., Crutcher, R. M., Girart, J. M., & Rao, R. 2001, *ApJ*, 561, 864
- Lai, S.-P., Crutcher, R. M., Girart, J. M., & Rao, R. 2002, *ApJ*, 566, 925
- Lai, S.-P., Girart, J. M., & Crutcher, R. M. 2003, *ApJ*, 598, 392
- Larson, R. B. 1969, *MNRAS*, 145, 271
- Larson, R. B. 1972, *MNRAS*, 157, 121
- Larson, R. B. 1981, *MNRAS*, 194, 809
- Lequeux, J. 1975, *A&A*, 39, 257
- Levermore, C. D., & Pomraning, G. C. 1981, *ApJ*, 248, 321
- McKee, C. F. 1989, *ApJ*, 345, 782
- Mac Low, M.-M., & Klessen, R. S. 2004, *Rev. Mod. Phys.*, 76, 125
- Mac Low, M.-M., Norman, M. L., Königl, A., & Wardle, M. 1995, *ApJ*, 442, 726
- Masunaga, H., Miyama, S. M., & Inutsuka, S.-i. 1998, *ApJ*, 495, 346
- Mathis, J. S., Rumpl, W., & Nordsieck, K. H. 1977, *ApJ*, 217, 425
- Mellon, R. R., & Li, Z.-Y. 2008, *astro-ph/0809.3593*
- Mestel, L. 1965, *QJRAS*, 6, 265
- Mestel, L. 1966, *MNRAS*, 133, 265
- Mestel, L., & Spitzer, L., Jr. 1956, *MNRAS*, 116, 503
- Mihalas, D., & Mihalas, B. W. 1984, *Foundations of Radiation Hydrodynamics* (New York: Oxford University Press)
- Morton, D. C. 1974, *ApJ*, 193, L35
- Mouschovias, T. Ch. 1976a, *ApJ*, 206, 753
- Mouschovias, T. Ch. 1976b, *ApJ*, 207, 141
- Mouschovias, T. Ch. 1977, *ApJ*, 211, 147
- Mouschovias, T. Ch. 1978, in *Protostars and Planets*, ed. T. Gehrels (Tucson: University of Arizona Press), 209
- Mouschovias, T. Ch. 1979, *ApJ*, 228, 159
- Mouschovias, T. Ch. 1987, in *Physical Processes in Interstellar Clouds*, ed. G. E. Morfill & M. Scholer (Dordrecht: Reidel), 453
- Mouschovias, T. Ch. 1991, *ApJ*, 373, 169
- Mouschovias, T. Ch. 1996, in *Solar and Astrophysical Magnetohydrodynamic Flows*, ed. K. Tsiganos (Dordrecht: Kluwer), 505
- Mouschovias, T. Ch., & Morton, S. A. 1991, *ApJ*, 371, 296
- Mouschovias, T. Ch., & Morton, S. A. 1992a, *ApJ*, 390, 144
- Mouschovias, T. Ch., & Morton, S. A. 1992b, *ApJ*, 390, 166
- Mouschovias, T. Ch., & Paleologou, E. V. 1979, *ApJ*, 230, 204
- Mouschovias, T. Ch., & Paleologou, E. V. 1980, *ApJ*, 237, 877
- Mouschovias, T. Ch., Paleologou, E. V., & Fiedler, R. A. 1985, *ApJ*, 291, 772
- Mouschovias, T. Ch., & Psaltis, D. 1995, *ApJ*, 444, L105
- Mouschovias, T. Ch., & Spitzer, L., Jr. 1976, *ApJ*, 210, 326
- Mouschovias, T. Ch., Tassis, K., & Kunz, M. W. 2006, *ApJ*, 646, 1043
- Myers, P. C. 1985, in *Protostars & Planets II*, ed. D. C. Black & M. S. Mathews (Tucson: University of Arizona Press), 81
- Myers, P. C., & Benson, P. J. 1983, *ApJ*, 266, 309
- Myers, P. C., & Gammie, C. F. 1999, *ApJ*, 522, L141
- Myers, P. C., Linke, R. A., & Benson, P. J. 1983, *ApJ*, 264, 517
- Nakano, T. 1979, *PASJ*, 31, 697
- Nakano, T., & Umebayashi, T. 1980, *PASJ*, 32, 613
- Nakano, T., & Umebayashi, T. 1986a, *MNRAS*, 218, 663
- Nakano, T., & Umebayashi, T. 1986b, *MNRAS*, 221, 319
- Nishi, R., Nakano, T., & Umebayashi, T. 1991, *ApJ*, 368, 181
- Novak, G., Dotson, J. L., Dowell, C. D., Goldsmith, P. F., & Hildebrand, R. H. 1997, *ApJ*, 487, 320
- Novak, G., Gonatas, D. P., Hildebrand, R. H., Platt, S. R., & Dragovan, M. 1989, *ApJ*, 345, 802
- Paleologou, E. V., & Mouschovias, T. Ch. 1983, *ApJ*, 275, 838
- Parks, G. K. 1991, *Physics of Space Plasmas* (Redwood City: Addison-Wesley), 283
- Pneuman, G. W., & Mitchell, T. P. 1965, *Icarus*, 4, 494
- Pollack, J. B., Hollenbach, D., Beckwith, S., Simonelli, D. P., Roush, T., & Fong, W. 1994, *ApJ*, 421, 615
- Preibisch, Sonnhalter, & Yorke, H. W. 1995, *A&A*, 299, 144
- Schleuning, D. A. 1998, *ApJ*, 493, 811
- Schleuning, D. A., Vaillancourt, J. E., Hildebrand, R. H., Dowell, C. D., Novak, G., Dotson, J. L., & Davidson, J. A. 2000, *ApJ*, 535, 913
- Scott, E. H., & Black, D. C. 1980, *ApJ*, 239, 166
- Snow, T. P., Jr. 1976, *ApJ*, 204, 759
- Spitzer, L., Jr. 1941, *ApJ*, 93, 369
- Spitzer, L., Jr. 1948, *ApJ*, 107, 6
- Spitzer, L., Jr. 1968, *Diffuse Matter in Space* (New York: Interscience)
- Spitzer, L., Jr. 1978, *Physical Processes in the Interstellar Medium* (New York: Wiley-Interscience)
- Stone, J. M., Mihalas, D., & Norman, M. L. 1992, *ApJS*, 80, 819
- Stone, J. M., & Norman, M. L. 1992, *ApJS*, 80, 753
- Strittmatter, P. A. 1966a, *MNRAS*, 131, 491
- Strittmatter, P. A. 1966b, *MNRAS*, 132, 359
- Tassis, K., & Mouschovias, T. Ch. 2005a, *ApJ*, 618, 769
- Tassis, K., & Mouschovias, T. Ch. 2005b, *ApJ*, 618, 783
- Tassis, K., & Mouschovias, T. Ch. 2007a, *ApJ*, 660, 370
- Tassis, K., & Mouschovias, T. Ch. 2007b, *ApJ*, 660, 388
- Tassis, K., & Mouschovias, T. Ch. 2007c, *ApJ*, 660, 402
- Troland, T. H., Crutcher, R. M., & Kazès, I. 1986, *ApJ*, 304, L57
- Troland, T. H., Crutcher, R. M., Goodman, A. A., Heiles, C., Kazès, I., & Myers, P. C. 1996, *ApJ*, 471, 302
- Tscharnuter, W. 1975, *A&A*, 39, 207
- Tscharnuter, W. 1978, *The Moon and the Planets*, 19, 229
- Tscharnuter, W. M., & Winkler, K.-H. A. 1979, *Comput. Phys. Comm.*, 18, 171
- Turner, N. J., & Stone, J. M. 2001, *ApJS*, 135, 95
- Umebayashi, T. 1983, *Prog. Theor. Phys.*, 69, 480
- Umebayashi, T., & Nakano, T. 1980, *PASJ*, 32, 405
- Umebayashi, T., & Nakano, T. 1990, *MNRAS*, 243, 103
- Vrba, F. J., Coyne, G. V., & Tapia, S. 1981, *ApJ*, 243, 489
- Watson, W. D. 1976, *Rev. Mod. Phys.*, 48, 513
- Whitehouse, S. C., & Bate, M. R. 2006, *MNRAS*, 367, 32
- Winkler, K.-H., & Newman, M. J. 1980a, *ApJ*, 236, 201
- Winkler, K.-H., & Newman, M. J. 1980b, *ApJ*, 238, 311
- Yorke, H. W. 1977, *A&A*, 58, 423
- Yorke, H. W. 1980, *A&A*, 85, 215
- Yorke, H. W., & Krugel, E. 1977, *A&A*, 54, 183
- Yorke, H. W., & Shustov, B. M. 1981, *A&A*, 98, 125
- Yorke, H. W., & Sonnhalter, C. 2002, *ApJ*, 569, 846
- Zuckerman, B., & Evans, N. J. 1974, *ApJ*, 192, L149
- Zweibel, E. G., & Josafatsson, K. 1983, *ApJ*, 270, 511